Cortical neurons obtained from patients-derived GNAO1 iPSCs show altered differentiation and functional properties

Maria Cristina Benedetti[1,2], Tiziano D'Andrea[3], Alessio Colantoni[1,2], Denis Silachev[4,5,6], Valeria de Turris[2], Zaira Boussadia[7], Valentina A. Babenko[5,6], Egor A. Volovikov[8,9], Lilia Belikova[8,9], Alexandra N. Bogomazova[8,9], Rita Pepponi[7], Dosh Whye[10], Elizabeth D. Buttermore[10], Gian Gaetano Tartaglia[11], Maria A. Lagarkova[8,9], Vladimir L. Katanaev[4,6], Ilya Musayev[12], Simone Martinelli[13], Sergio Fucile[3,14] and Alessandro Rosa[1,2,*]

1. Department of Biology and Biotechnologies "Charles Darwin", Sapienza University of Rome, Rome, Italy.
2. Center for Life Nano- & Neuro-Science, Fondazione Istituto Italiano di Tecnologia (IIT), Rome, Italy.
3. Department of Physiology and Pharmacology "V. Erspamer", Sapienza University of Rome, Rome, Italy.
4. Institute of Life Sciences and Biomedicine, Far Eastern Federal University, 690090, Vladivostok, Russia.
5. A.N. Belozersky Research Institute of Physico-Chemical Biology, Moscow State University, 119992, Moscow, Russia.
6. Department of Cell Physiology and Metabolism, Faculty of Medicine, Translational Research Center in Oncohaematology, University of Geneva, 1211, Geneva, Switzerland.
7. National Center for Drug Research and Evaluation, Istituto Superiore di Sanità, Rome, Italy.
8. Lopukhin Federal Research and Clinical Center of Physical-Chemical Medicine of Federal Medical Biological Agency, 119435 Moscow, Russia.
9. Center for Precision Genome Editing and Genetic Technologies for Biomedicine, Federal Research and Clinical Center of Physical-Chemical Medicine of Federal Medical Biological Agency, 119435 Moscow, Russia
10. Human Neuron Core, Rosamund Stone Zander Translational Neuroscience Center and F.M. Kirby Neurobiology Department, Boston Children's Hospital, Boston, Massachusetts, USA.

11. Center for Human Technologies (CHT), Istituto Italiano di Tecnologia (IIT), Genova, Italy.
12. Child's Cure Genetic Research, Fremont, California, USA.
13. Department of Oncology and Molecular Medicine, Istituto Superiore di Sanità, Rome, Italy.
14. IRCCS Neuromed, Pozzilli, Italy.

* Correspondence: alessandro.rosa@uniroma1.it

ABSTRACT

Pathogenic variants in the *GNAO1* gene, encoding the alpha subunit of an inhibitory heterotrimeric guanine nucleotide-binding protein (Go) highly expressed in the mammalian brain, have been linked to encephalopathy characterized by different combinations of neurological symptoms, including developmental delay, hypotonia, epilepsy and hyperkinetic movement disorder with life-threatening paroxysmal exacerbations. Currently there are no curative but only symptomatic treatments, and little is known on the pathophysiology of the disease. In this work, we report the characterization of a new *in vitro* model system based on patient-derived induced pluripotent stem cells (iPSCs) carrying the recurrent p.G203R amino acid substitution in Gαo, and a CRISPR-Cas9-genetically corrected isogenic control line. RNA-Seq analysis highlighted aberrant cell fate commitment in neuronal progenitor cells carrying the p.G203R pathogenic variant. Upon differentiation into cortical neurons, patients' cells showed reduced expression of early neural genes and increased expression of astrocyte markers, as well as premature and defective differentiation processes leading to aberrant formation of neuronal rosettes. Of note, comparable defects in gene expression and in the morphology of neural rosettes were observed in hiPSCs from an unrelated individual harboring the same *GNAO1* variant. Functional characterization showed lower basal intracellular free calcium concentration ($[Ca^{2+}]_i$), reduced frequency of spontaneous activity, and a smaller response to several neurotransmitters in 40- and 50-days differentiated p.G203R neurons compared to control cells. These findings suggest that the *GNAO1* pathogenic variant causes a neurodevelopmental phenotype characterized by aberrant differentiation of both neuronal and glial populations leading to a significant alteration of neuronal communication and signal transduction.

INTRODUCTION

The *GNAO1* gene, encoding the alpha-o1 subunit of guanine nucleotide-binding protein (Gαo), has been recently associated to Developmental and Epileptic Encephalopathies (DEE), a clinically and genetically heterogeneous group of neurological disorders with onset during infancy or childhood (Nakamura et al., 2013). Pathogenic variants in the *GNAO1* gene cause encephalopathy affecting psychomotor development with high clinical heterogeneity, including developmental delay, intellectual disability, early-onset hyperkinetic movement disorders with severe exacerbations, epileptic seizures and prominent hypotonia. It was first described in patients with early infantile epileptic encephalopathy 17 (EIEE17, MIM #615 473) (Nakamura et al., 2013). Later *GNAO1* variants were reported in patients affected by neurodevelopmental disorder with involuntary movements, with or without epilepsy (NEDIM, MIM #617 493) (Ananth et al., 2016). Approximately 50 pathogenic variants have been reported so far (www.ncbi.nlm.nih.gov/clinvar/). Most of them are missense changes in highly conserved residues spread across the entire length of the protein. Codons 203, 209 and 246 represent mutational hotspots, occurring in about 50% of cases. A different class of variants leading to *GNAO1* haploinsufficiency has recently been associated with a relatively mild and delayed-onset dystonia phenotype (Wirth et al., 2022; Krenn et al., 2022). Despite the increasing number of children diagnosed with GNAO1 encephalopathy, no effective cure or treatment are available.

Gαo is the most abundant membrane protein in the mammalian central nervous system, playing major roles in neurodevelopment (Jiang et al., 1998) and neurotransmission (Wettschureck and Offermanns, 2005). In the brain, Go controls the synthesis of cAMP modulating inhibitory and stimulatory inputs to the adenylyl cyclase 5 (ADCY5) (Muntean et al., 2021). It mediates inhibitory signaling downstream to several neurotransmitters, including dopamine, adenosine and GABA, through inhibition of calcium channel (Colecraft et al., 2001; McDavid et al., 2006) or by preventing neurotransmitter release (Zamponi et al., 2013). It is ubiquitously expressed in the central nervous system, but it is highly enriched in the cerebral cortex, hippocampus and striatum (Worley et al., 1986).

Little is known about the molecular mechanism that triggers the neurodevelopmental phenotype in patients carrying pathogenic *GNAO1* variants. Recent studies on different animal models paved the way to a deeper understanding of this pathology. These include mouse, Drosophila and *C. elegans* (Larrivee et al., 2020; Silachev et al., 2022; Savitsky et al., 2020; Larasati et al., 2022; Wang et al., 2022, Di Rocco et al., 2022, Di Rocco et al.,

2023). However, species-specific differences (e.g. neonatal lethality in p.G203R/+ mice; Silachev et al., 2022) make it hard to translate findings from animal to human, hence the necessity for more reliable models. In this regard, human induced pluripotent stem cells (hiPSCs) represent a valuable tool for disease modeling and drug screening since they can be derived directly from patients and then differentiated ideally in any cell type of interest. Moreover, gene editing allows the introduction of specific nucleotide substitutions in existing iPSC lines from healthy individuals, generating pairs of mutated/wild-type isogenic lines.

Here we report the characterization of a new hiPSC-based *in vitro* model of GNAO1 encephalopathy. We have generated cortical neurons from hiPSCs derived from a patient carrying the p.G203R amino acid change and performed molecular, cellular and functional studies at different time points during differentiation. Importantly, all experiments have been carried out in parallel on an isogenic *GNAO1* wild-type line generated by reverting the mutation by CRISPR-Cas9-mediated gene editing. Compared to such appropriate control, GNAO1-G203R cells show altered expression of early and late key differentiation genes, altered timing of differentiation and increased number of astrocytes, and functional impairment. The altered gene expression and differentiation of neuronal precursor cells was confirmed in a second hiPSC line derived from an unrelated individual harboring the p.G203R *GNAO1* variant.

RESULTS

RNA-Seq analysis reveals impaired neuronal fate commitment in GNAO1 p.G203R neural progenitor cells

HiPSCs derived form an American patient and isogenic control hiPSCs generated by gene editing have been provided by Child's Cure Genetic Research (see Methods section). In this work, such lines are referred to as GNAO1$^{+/G203R}$ and GNAO1$^{+/G203G}$, respectively (Figure 1A).

We first analysed RNA-Seq data previously obtained from hiPSC-derived neural progenitor cells (NPCs; day 7 and day 11 of differentiation; n=3 replicates from one differentiation batch). By performing differential gene expression (DGE) analysis we detected, in GNAO1$^{+/G203R}$ NPCs compared to GNAO1$^{+/G203G}$ NPCs, 3,451 downregulated genes and 3,372 upregulated genes at day 7, while 4,174 genes were downregulated and 5,081

genes were upregulated at day 11 (adjusted *p*-value < 0.01) (Supplementary Table S1). These results suggest that at early phases of neural induction the G203R variant has an extensive impact on gene expression, as also indicated by principal component analysis (PCA) (Supplementary Figure S1A), showing that the transcriptional profile clearly segregates samples, exhibiting distinct patterns that can be attributed not only to their differentiation stage but also to their genotype. Such effects of the mutation on gene expression are particularly evident at day 11. We observed a good overlap between the sets of genes that exhibited deregulation upon *GNAO1* mutation at day 7 and day 11; however, the expression of several genes changed in opposite directions (Supplementary Figure S1B). Gene Set Enrichment Analysis (GSEA) indicated that downregulated genes are enriched in those involved in cell fate commitment, many of which control neuronal differentiation (Figure 1B). Among them, we noticed well-known neural progenitors (*PAX6*, *NES/NESTIN*, *EOMES/TBR2*, *CDH2*, *OTX1*) and neuronal markers (*CUX1*), while astrocyte markers were mostly upregulated (Figure 1C). In general, GSEA showed that deregulated genes are involved in many biological processes related to neural differentiation (Supplementary Figure S2A). Specifically, we observed extensive downregulation of genes related to neurodevelopmental processes, such as “forebrain development”, “neuron migration,” “central nervous system”, “neuron differentiation” and “hindbrain development”. We also observed a downregulation of WNT pathway components (Jassal et al., 2020), particularly on day 7, and to a somewhat lesser extent on day 11 (Figure 1B; Supplementary Figure S2B,C). Notably, this pathway regulates neurogenesis and gliogenesis in the cortex with a specific temporal gradient, and downregulation of WNT signalling has been shown to reduce the timing of neurogenesis and trigger precocious astrogenesis (Bem et al., 2019). Further, Gαo can act as a direct transducer of the WNT-Frizzled signaling (Katanaev et al., 2005; Koval and Katanaev, 2011), reinforcing the importance of our findings that components of this pathway are downregulated in GNAO1$^{+/G203R}$ NPCs.

Collectively, RNA-Seq data suggest that during early neurogenesis the *GNAO1* p.G203R pathogenic variant affects cell fate commitment, and in particular neuronal fate, causing the downregulation of genes implicated in neurodevelopment and, on the other hand, the upregulation of astrocyte markers.

GNAO1 p.G203R hiPSCs show impaired neuronal differentiation

GNAO1$^{+/G203R}$ hiPSCs, along with the isogenic GNAO1$^{+/G203G}$ control line, were differentiated into cortical neurons using a method previously described (Brighi et al., 2021), based on dual SMAD inhibition followed by the inhibition of SHH signalling with cyclopamine to induce a neural cortical fate (Figure 2A). This protocol recapitulates the steps of neural induction during embryonic development, including the formation of neural rosettes that mimic *in vitro* the forming neural tube. At day 25 of differentiation, when control cells showed the typical radial organization of neural progenitors in rosettes, GNAO1$^{+/G203R}$-derived cells did not acquire such morphology and showed a more advanced phenotype (Figure 2B). Impaired timing of differentiation was confirmed by gene expression analysis performed by qRT-PCR, showing altered levels of neural progenitor markers, such as *NESTIN*, *OTX2* and *PAX6* in patient-derived cells compared to the isogenic control (Figure 2C), in agreement with RNA-Seq analysis at earlier time points (Figure 1B). GNAO1$^{+/G203R}$ cells also expressed lower levels of *TBR2* and *TBR1*, that in the developing neocortex are expressed in intermediate progenitor cells and postmitotic neurons, respectively (Englund et al., 2005), agreeing with the reduced numbers of TBR1- and TBR2-positive cells in the cortex of mice harboring pathogenic GNAO1 mutations (Silachev et al., 2022). These results were further confirmed by immunostaining analysis at the same time point, showing a reduced number of PAX6-, TBR2- and NESTIN-positive progenitors in patient-derived cells compared to the isogenic control (Figure 3).

Analysis of the neural rosettes of a Russian patient with the GNAO1$^{+/G203R}$ variant (herafter GNAO1$^{+/G203R}$#2) showed similar violations in the morphology of the neural rosettes. GNAO1$^{+/G203R}$#2 hiPSCs, along with the control cell line from a healthy donor, were differentiated into cortical neurons using a method previously described (Vigont et al., 2021). Neural rosette formation was examined on day 30 of differentiation in both control and mutant cultures. The control cultures exhibited cellular rosettes formed by the accumulation of several tens to hundreds of cells, whereas the mutant cultures showed clusters of only 10-20 cells (Figure 4A,B). Immunocytochemical analysis of the neuronal markers TBR1, TUJ1 (Figure 4B), and MAP2 (Figure 4C) revealed the presence of positively stained cells at the edge of the neural rosettes in the control culture. In contrast, the number of these cells was significantly lower in the mutant culture (Figure 4B,C). Similarly, a marked reduction in NESTIN-positive progenitor cells was observed in the mutant culture compared with the controls (Figure 4C). In addition, the mutant rosettes exhibited disrupted cytoarchitecture, a lack of cell polarization, and the absence of radial

structure. Apical polarization of β-catenin was also impaired in the mutant culture (Figure 4D).

Collectively these data suggest an early impairment that affects *GNAO1* p.G203R neural progenitor cells. Importantly, morphologic abnormalities in neural rosettes were consistently observed in two independent patient-derived *GNAO1* p.G203R lines.

The GNAO1 p.G203R substitution alters neuronal maturation

At day 40, corresponding to a stage in which differentiated cells have entered the neuronal maturation stage, GNAO1$^{+/G203R}$-derived neurons continued to express lower levels of *TBR1*, which highlights a reduction in the presence of VI layer neurons (Figure 5A,B). On the other hand, they tended to express higher levels of *GFAP*, an astrocyte marker, compared to the isogenic control, and failed to downregulate *PAX6* expression, suggesting a higher amount of astrocyte and progenitor cells (Figure 5A,B). Furthermore, the expression levels of *FOXG1*, a telencephalic gene that plays an important role in neural differentiation and in balancing the excitatory/inhibitory network activity, were increased (Figure 5A). At later time points (day 50 and day 70), we confirmed significant *TBR1* downregulation in mutant neural cultures, whereas we observed an increased trend of upregulation for *GFAP* (at both day 50 and day 70), *PAX6* (day 50, not tested at day 70) and *FOXG1* (only at day 50), despite statistical significance is not always reached (Figure 6A-C).

Collectively, these findings indicate that the *GNAO1* p.G203R variant leads to altered gene expression as well as premature and defective differentiation processes affecting both neurons and astrocytes.

Spontaneous and evoked Ca^{2+} transients were reduced in GNAO1-G203R cortical neurons

Functional characterization was performed on days 40 and 50 by taking advantage of calcium imaging. As shown in Figures 7 and 8, this analysis suggests impaired functional maturation in neuronal cultures obtained from patient-derived GNAO1$^{+/G203R}$ iPSCs. At both time points, mutated cultures showed decreased levels of basal intracellular free calcium concentration ($[Ca^{2+}]_i$) and a reduced fraction of neurons with spontaneous activity (Figure 6B). In line with this finding, calcium-dependent signalling was affected in 50-days differentiated GNAO1$^{+/G203R}$ neurons, which displayed lower levels of pGSK3β at the inhibitory Ser9 residue than control cells (Supplementary Figure S3). We then tested the

response of control and mutant neurons to different neurotransmitters or selective agonists. The highest response levels were obtained, both in control and mutated neurons, upon application of glutamate (Figure 8A), but with a significant decrease in the percentage (at day 40) and in the amplitude of the responses in mutated neurons (at both time points). The most striking difference was detected upon stimulation with GABA (Figure 8B). While the vast majority of wild-type neurons responded to GABA stimulation at both time points, this effect was almost completely abolished by the mutation. Moreover, the amplitude of the $[Ca^{2+}]_i$ increase was significantly lower even in the few $GNAO1^{+/G203R}$ cells able to respond to GABA. We also tested baclofen, a specific agonist of $GABA_B$ receptors (Figure 8C). In this case, we observed a statistically significant difference only in the number of responding cells at day 50. Reduced activity did not correlate with a decrease in GABBR2 ($GABA_B$ Receptor 2) and GRIA4 (Glutamate Ionotropic Receptor AMPA Type Subunit 2) mRNA levels (Figure 5A), pointing to functional impairment rather than decreased expression of receptors. Reduced activity in response to other neurotransmitters, such as glycine, acetylcholine, and ATP was also observed in terms of the number of responding cells (Figure 8D-F). These results suggest that the *GNAO1* p.G203R variant leads to a delay in neuronal maturation, which in turn causes a profound impairment of neuronal function.

DISCUSSION

Since a link between *GNAO1* mutations and rare DEEs was reported for the first time a decade ago (Nakamura et al., 2013), several animal models have been raised to understand the pathophysiology of the *GNAO1*-related neurodevelopmental disorder. Knockout models suggest that *GNAO1* plays a pivotal role both in both adult brain and during early neurogenesis. Its expression indeed increases during axonogenesis, knockout mice show impaired neurogenesis while a *Gnao1* mutated Drosophila model shows defects during axon guidance (Guillén et al., 1991; Wolfgang et al., 1991; Fremion et al., 1999). *GNAO1* disease-linked pathogenic variants in mouse and worm models lead to a loss of function in Gα-mediated signaling with or without a dominant negative effect (Muntean et al., 2021; Wang et al., 2022; Di Rocco et al., 2022; Di Rocco et al., 2023).

To the best of our knowledge, there is only one hiPSC-based study of GNAO1 disease (Akamine et al., 2020). The authors showed abnormal structure and aberrant neurite outgrowth in GNAO1-KO spheroids (Akamine et al., 2020). They assessed a defect in

lamination and found few neural rosettes and the loss of PAX6 expression compared to wild-type (WT) cells. They confirmed some of these findings in patient hiPSCs carrying the p.G203R substitution. However, a major limitation of this study is the lack of proper isogenic *GNAO1* WT control for the patient-derived line. Comparison of mutated lines with their isogenic counterpart, indeed, is crucial to distinguish between phenotypes due to the presence of the mutation from those originating from different genetic backgrounds (Soldner et al., 2011; Sandoe and Eggan, 2013; Vasques et al., 2020). Here we provide a side-by-side comparison of patient-derived hiPSCs and a proper control in which the p.G203R change has been reverted to WT ($GNAO1^{+/G203G}$). The highly conserved glycine 203 residue represents a mutational hotspot, associated with a mixed, severe phenotype characterized by epileptic seizures and movement disorder (Saitsu et al., 2016; Danti et al., 2017). Together with glutamic acid 246 and arginine 209, this residue plays a crucial role in the allosteric regulation mediating Gβγ release (Knight et al., 2021). The core molecular dysfunction for the three most common *GNAO1* pathogenic variants (p.G203R, p.R209C/H, and p.E246K) is the constitutive GTP-bound state of the mutant Gαo proteins coupled to their inability to adopt the active conformation which allow proper binding to regulators and effectors (Larasati et al., 2022). Indeed, these three residues are located in the switch II or switch III regions, important for guanidine nucleotide-dependent regulation of downstream effectors.

In this work the $GNAO1^{+/G203R}$ hiPSC line from an American patient and its $GNAO1^{+/G203G}$ isogenic control were differentiated into cortical neurons using a method that properly recapitulates human corticogenesis. The comparison with the isogenic control shows that p.G203R is sufficient to impair proper differentiation as early as at day 25, representing the onset of neuronal differentiation from neural progenitor cells. Similar impairment in the ability to form neural rosettes was consistently observed in a second $GNAO1^{+/G203R}$ line derived from an unrelated Russian patient. This agreement confirms the importance of the hiPSCs *GNAO1* model in elucidating the pathogenesis of the disease and underscores the importance of further investigation of the role of this mutation in the pathogenesis of GNAO1 encephalopathy.

In line with these results, we have recently shown a decrease of neural progenitor cells in two different mouse models of GNAO1 encephalopathy (p.C215Y and p.G203R), suggesting an impairment in neuronal differentiation or migration, specifically in the developing cerebral cortex (Silachev et al., 2022). We found enlargement of lateral ventricles and altered motor cortex thickness. We also reported a reduction of cell number

in the total cortex, while no change was observed in the striatum and hippocampus. Accordingly, here we show that compared to the isogenic control line, human GNAO1-G203R differentiating neural progenitors are characterized by reduced expression of early neural genes, such as *NESTIN*, *OTX2* and *PAX6*. Moreover, in line with the mouse model which has halved *tbr2*-positive cells in the ventricular and subventricular zone and a lower cell density in layer VI of the cortex (*tbr1*-positive cells) (Silachev et al., 2022), here we found decreased levels of both *TBR1* and *TBR2* transcripts. Altered expression of *FOXG1*, which was significantly upregulated at day 40 and shows the same trend at later time points, is intriguing. Indeed, mutations in the *FOXG1* gene have been linked to a rare form of epileptic encephalopathy (Wong et al., 2019). *TBR1* is a master regulator of cortex development that plays a crucial role in the formation of neocortical layer VI, regulating both neuronal migration and synaptic development (Darbandi et al., 2018; Crespo et al., 2022). Mutations in *TBR1* gene are associated with cortical malformations, intellectual disability and autism spectrum disorder. On the other hand, we report increased expression of *GFAP*, an intermediate progenitor marker expressed in astrocytes. *GFAP* overexpression has been found both in neurodevelopmental and neurodegenerative disease, as FXS and AD (Pacey et al., 2015; Sunamura et al., 2018; Brighi et al., 2021; Chatterjee et al., 2021; Ganne et al., 2022), and is considered as a hallmark of reactive astrocytes, which are astrocytes that underwent through morphological and functional modification as a consequence of brain injury or disease (Escartin et al 2021), suggesting that *GNAO1* pathogenic variants could have an effect both on neuronal and glial population.

Our functional analysis supports the concept that the *GNAO1* p.G203R substitution leads to a lower degree of neuronal maturation. Control neurons exhibit a sustained spontaneous $[Ca^{2+}]_i$ activity, which is significantly reduced in mutated cells, in association with a reduction of the basal $[Ca^{2+}]_i$. As a probable consequence of the decrease in $[Ca^{2+}]_i$, we found lower levels of pGSK3β(S9) in 50-days differentiated p.G203R neurons compared to control cells, which is in line with previous findings in neuronal cultures knockout for the *GNAO1* gene or carrying the *GNAO1* p.G203R variant (Akamine et al., 2020). Considering the key role of Wnt-GSK3 signaling in the regulation of axon extension and branching (Kim et al., 2011), further studies are needed to explore the impact of aberrant GSK3β phosphorylation in p.G203R neuronal morphogenesis. Furthermore, mutated neurons are less responsive to several agonists, indicating a lower functional level of different crucial receptor systems. In particular, both GABA and glutamate induce a

much lower response in mutated neurons, suggesting a profound impairment of the neuronal function in the presence of the mutated Gαo in 40-days and 50-days differentiated p.G203R neurons compared to control cells.

Overall, our findings provide new evidence indicating that GNAO1 encephalopathy is a neurodevelopmental disorder. Further studies are warranted to explore the functional consequences of the p.G203R variant in fully matured neurons, as well as of other *GNAO1* pathogenic variants associated with diverse clinical features.

MATERIALS AND METHODS

Reprogramming of patient-derived hiPSCs and generation of the gene edited GNAO1$^{+/G203G}$ control line

GNAO1$^{+/G203R}$ iPSCs derived from an American patient and the isogenic control line were kindly provided by the nonprofit organization Child's Cure Genetic Research (Fremont, CA, USA). Briefly, fibroblasts were derived at the Stanford Children's Hospital (CA, USA) from a skin punch biopsy of a GNAO1$^{+/G203R}$ patient (male, 2 years old at the time of biopsy). Reprogramming to iPSCs, followed by standard characterization, was performed by Applied StemCell Inc. The isogenic control line was generated using CRISPR/Cas9-mediated genome editing by the Genome Engineering & Stem Cell Center (GESC@MGI) at Washington University in St. Louis (https://GeneEditing.wustl.edu).

GNAO1$^{+/G203R}$#2 hiPSCs were generated by reprogramming of skin fibroblasts from a 1-year-old male patient from Moscow with GNAO1 encephalopathy carrying the c.607 G>A (p.Gly203Arg) variant were described in (Lunev et al., 2022), which were kindly provided by Dr. Bardina (Institute of Gene Biology, Russian Academy of Sciences, Moscow) upon the proper written patient consent. To generate control fibroblasts, a skin biopsy was obtained from a healthy 26-year-old female donor after informed consent. The biopsy was cut into small pieces and cultured under the coverslip in DMEM (PanEco, Russia) with 10% FBS (Hyclone, USA), 2 mM Glutamine (PanEco), 1X penicillin-streptomycin (PanEco). Medium was changed once in three days. After seven days, fibroblasts were passaged with 0.25% Trypsin (Gibco). Human skin fibroblasts from the patient and the healthy donor were reprogrammed using the CytoTune™-iPS 2.0 Sendai Reprogramming Kit (ThermoFisher Scientific, USA). Cells were transduced with the Sendai reprogramming vectors at the individual MOI 5. Infected cells were transferred with 0.05% trypsin on

Matrigel (Corning, USA) 1:5 by area. Then the cells were cultured in human pluripotent cell culture medium (DMEM/F12, 20% serum replacement, 2 mM glutamine, 0.1 mM β-mercaptoethanol, 1% non-essential amino acids, bFGF 10 ng/mL, penicillin-streptomycin (50 U/mL; 50 µg/mL). The cell medium was changed every day. On day 15, the selection of clones was started, based on the morphological criteria of similarity of colonies with human ESCs colonies. After 2-4 passages, the iPSCs were transferred to the mTeSR 1 and then TeSR-E8 (Stem Cell Technologies, USA) medium on a Matrigel substrate (Corning).

RNA-Sequencing and bioinformatic analysis

FASTQ files from paired-end RNA-Seq analysis performed using the Illumina® Stranded Total RNA Prep kit with Ribo-Zero Plus treatment on GNAO1$^{+/G203R}$ and GNAO1$^{+/G203G}$ hiPSC-derived NPCs at day 7, generated at Rarebase PBC, and day 11, generated as previously described in Whyte et al. (2023) (basic protocol 1 and support protocol 3). For each time point, 3 replicates from one differentiation batch were used. Raw RNA-Seq datasets were provided by Child's Cure Genetic Research. Forward and reverse reads were aligned to a database of rRNA sequences using Bowtie 2 v2.4.4 (Langmead and Salzberg, 2012) with --nofw and --nofw parameters, respectively; only read pairs in which both mates did not map to these abundant molecules were retained for downstream analyses. STAR v2.7.10b (Dobin et al., 2013) with default mapping parameters was used to align reads to the human GRCh38 genome, providing the GENCODE 42 (Harrow et al., 2012) GTF file to generate a splice junction database and to calculate gene-level read counts with the --quantMode TranscriptomeSAM GeneCounts option. Read counts reported in the fourth column of ReadsPerGene.out.tab files were combined into a count matrix using a custom Python script. This matrix was used to calculate normalized expression values, expressed as FPKM (Fragments Per Kilobase of exon per Million mapped reads), using the "fpkm" function from the DESeq2 v1.34.0 R package (Love et al., 2014). We retained only protein-coding or lncRNA genes with FPKM > 0.5 in at least three samples for subsequent analysis. Prior to performing PCA using the DESeq2 "plotPCA" function, we applied regularized-log (rlog) transformation to the count data. To identify genes which are differentially express (DEGs) between GNAO1$^{+/G203R}$ and GNAO1$^{+/G203G}$ samples at both time points, Wald test with independent filtering was performed using the "DESeq" function. Apeglm method (Zhu et al., 2019) was employed for log2(fold change) shrinkage. The FDR-adjusted p-value threshold to select DEGs was

set to 0.01. Additionally, in both contrasts, we only selected genes that had an average FPKM greater than 0.5 in at least one of the two conditions being compared. The intersections between the DEGs identified in the two comparisons were visualized using the UpSetR v1.4.0 R package (Conway et al., 2017). Gene expression heatmaps were generated with the ComplexHeatmap v2.10 R package (Gu et al., 2016) using row-scaled (Z-score), rlog-transformed count data. The WebGestaltR v0.4.4 R package (Liao et al., 2019) was employed to perform Gene Set Enrichment Analysis (GSEA), using shrunken log2(fold change) values as a ranking metric.

HiPSC culture and differentiation

GNAO1$^{+/G203R}$ iPSCs were cultured in Nutristem-XF (Biological Industries) supplemented with 0.1% Penicillin-Streptomycin (Thermo Fisher Scientific) onto hESC-qualified Biolaminin 521 LN (Biolamina) functionalized plates. The culture medium was refreshed every day and cells were passaged every 4–5 days using 1 mg/mL Dispase II (Thermo Fisher Scientific). Cells were routinely tested for mycoplasma contamination. GNAO1$^{+/G203R}$ hiPSCs were differentiated into cortical neurons as previously described (Brighi et al., 2021). Briefly, hiPSCs were treated with Accutase (Thermo Fisher Scientific) and the single-cell suspension was plated in Biolaminin 521 LN-coated dishes at a seeding density of 100,000 cells per cm^2, in Nutristem-XF supplemented with 10 µM ROCK inhibitor. The day after seeding the medium was changed to N2B27 medium consisting of DMEM-F12, Dulbecco's Modified Eagle's Medium/ Nutrient Mixture F-12 Ham (Merck Life Sciences), Neurobasal Medium (Thermo Fisher Scientific), 1X N2 supplement (Thermo Fisher Scientific), 1X GlutaMAX (Thermo Fisher Scientific), 1X MEM-NEAA (Thermo Fisher Scientific), 1X B27 (Thermo Fisher Scientific), 1X Penicillin-Streptomycin (Thermo Fisher Scientific). This was considered as day 0 (D0). At this stage, SMAD inhibitors, 10 µM SB431542 and 500 nM LDN-193189 (Cayman Chemical), were added daily to induce neural fate. After 10 days, the uniform neuroepithelial sheet was broken into clumps of approximately 500 cells/clump and re- plated onto 1X poly-L-ornithine/laminin (Merck Life Sciences) coated dishes in N2B27 medium. At day 20, cells were dissociated using Accutase and plated onto poly-L-ornithine/laminin-coated dishes at a density of 100,000 cells per cm^2 in N2B27 medium supplemented with 10 µM ROCK inhibitor for the first 24 h. Culture medium was changed three times a week. At day 27, 2 µM Cyclopamine (Merck Life Sciences) was freshly added to N2B27 medium for 4 days. At day 30 to 35, immature neurons were dissociated using Accutase and re-plated into

poly-L-ornithine/laminin-coated dishes at a density of 100,000 cells per cm^2 in N2B27 medium supplemented with 20 ng/mL BDNF (Merck Life Sciences), 20 ng/mL GDNF (Peprotech), 20 ng/mL ascorbic acid (Merck Life Sciences), 1 mM cyclic AMP (Sigma Aldrich), and 5 µM DAPT (Adipogen Life Sciences).

GNAO1$^{+/G203R}$#2 hiPSCs were cultured in mTeSR™1 medium (Stem Cell Technologies) on Matrigel (Corning)-coated plates following the manufacturer's guidelines. Every day, the culture medium was renewed, and cells were passaged every 4-5 days up to 70-85% confluency utilizing 0.5 mM EDTA (Thermo Fisher Scientific). On the first day post-subculturing, cells were cultured in medium supplemented with 5 µM of the ROCK inhibitor StemMACS™ Y27632 (Miltenyi Biotec). The differentiation of hiPSCs into midbrain neurons was performed as previously described (Vigont et al., 2021). The differentiation of GNAO1$^{+/G203R}$#2 hiPSCs into mature human neurons comprised three main stages: (1) hiPSC differentiation into neuronal progenitor cells (NPCs); (2) expansion and maturation of NPCs; and (3) differentiation of NPCs into mature neurons. In brief, hiPSCs were differentiated into NPCs using the commercially available PSC Neural Induction Medium (Thermo Fisher Scientific) following the manufacturer's guidelines. This was considered as day 0 (D0). After 10 days of induction to NPCs, cells were detached from the substrate with 0.5 mM EDTA and were plated at density of 250,000-400,000 cells per cm^2 in Petri dishes or multi-well plates coated with Matrigel. Further cultivation took place in the medium for expansion and maturation of NPCs consisting of advanced DMEM/F12 (Thermo Fisher Scientific), Neurobasal Medium (Thermo Fisher Scientific), 2% Neural Induction Supplement (GIBCO). The ROCK inhibitor Y27632 5 µM was used for every seeding overnight with the following replace to the medium without ROCK inhibitor. After 18 days the differentiation protocol for maturation into neurons was initiated. Neural precursors were cultured and frozen until the third passage. We reseeded neural precursors to a density of 300,000-400,000 cells per cm^2. NPCs were seeded into wells coated with Matrigel and cultured in the medium containing DMEM/F12 (Thermo Fisher Scientific), 1X GlutaMAX (Thermo Fisher Scientific), 2% B27 (Thermo Fisher Scientific), 1X Penicilin-Streptomicin (Thermo Fisher Scientific), BDNF 20 ng/mL (GenScript), GDNF 20 ng/mL (GenScript), 200 µM ascorbic acid (Sigma Aldrich), 4 µM forskolin (Sigma Aldrich) for 2 weeks with subculturing during the first week. The ROCK inhibitor was used every passage overnight with the following replacement to the medium without the ROCK inhibitor.

Real-time PCR

Total RNA was extracted with the EZNA Total RNA Kit I (Omega Bio-Tek) and retrotranscribed using the iScript Reverse Transcription Supermix for RT-qPCR (Bio-Rad). Real-time RT-PCR was performed with iTaq Universal SYBR Green Supermix (Bio-Rad) on a ViiA 7 Real-Time PCR System (Applied Biosystems). The cDNA of the housekeeping gene ATP5O (ATP synthase, H^+ transporting, mitochondrial F1 complex, O subunit), used as internal control. A complete list of primers is provided in Supplementary material (Supplementary Table S2).

Immunostaining

GNAO1$^{+/G203R}$ differentiating cells were fixed in 4% paraformaldehyde solution (Merck Life Sciences) for 15 min at room temperature and washed twice with 1X phosphate buffer solution (PBS; Thermo Fisher Scientific). Fixed cells were permeabilized with PBS containing 0.2% Triton X-100 (Merck Life Sciences) for 15min and blocked with a solution containing 0.2% Triton X-100 and 5% Goat Serum (Merck Life Sciences) for 20 min at room temperature. Cells were then incubated overnight at 4 °C with primary antibodies at the following dilutions: mouse anti-PAX6 (sc81649 Santa Cruz Biotechnology, 1:50), mouse anti-GFAP (MAB360 Merck Life Sciences, 1:500), chicken anti-MAP2 (ab5392 Abcam, 1:2000), rabbit anti-β-TUBULIN III (TUJ1) (T2200 Merck Life Sciences, 1:2000), Rabbit Anti-Nestin (MA5-32272 Thermo Fisher Scientific, 1:100), Rabbit Anti-TBR2 (ab15894 Millipore,1:50). The day after, the primary antibody solution was washed out and cells were incubated with secondary antibodies for 1h at room temperature in the dark. AlexaFluor secondary antibodies (Thermo Fisher Scientific) were used at the concentration of 1:250, and DAPI (Merck Life Sciences) was used for nuclei staining. Images were acquired with an inverted Olympus iX73 equipped with an X-Light V3 spinning disc head (Crest Optics), a LDI laser illuminator (89 North) using 405nm, 470nm, 555nm and 640nm wavelengths, depending on the fluorophores, a Prime BSI sCMOS camera (Photometrics) and MetaMorph software (Molecular Devices) with a 20x objective (Olympus).

GNAO1$^{+/G203R}$#2 cells at the stage of neuronal rosettes (30 day of differentiation) were fixed in 4% paraformaldehyde solution (Merck Life Sciences) for 15 min at room temperature and washed thrice with 1X PBS (Thermo Fisher Scientific). Fixed cells were permeabilized for 1 min using ice-cold PBS supplemented with 0.1% Triton X-100, blocked for 30 min with PBS supplemented with 1% BSA. Cells were then incubated overnight at

4°C with primary antibodies at the following dilutions: rabbit anti-MAP2 (ab254264 Abcam, 1:2000), mouse anti-βTUBULIN III (TUJ1) (T8660 Sigma-Aldrich, 1:500), mouse Anti-Nestin (ab6142 Abcam, 1:250), rabbit anti-TBR1 (ab183032 Abcam,1:200), mouse anti-β-Catenin (571-781 BD Transduction Laboratories, 1:200). The day after, the primary antibody solution was washed out and the cells were incubated with secondary antibodies (Alexa Fluor 488 or Alexa Fluor 594 conjugates, Jackson ImmunoResearch, 1:250) for 2 h at room temperature in the dark. DAPI (Merck Life Sciences) was used for nucleus staining. Images were acquired with an LSM710 confocal microscope.

Western Blotting

Differentiating cells were lysed with RIPA Buffer with freshly added protease and phosphatase inhibitors (Thermo Fisher Scientific), and kept on ice for 30 min. Afterwards they were centrifuged at 12.000×g (20 min, 4 °C), the pellet was discarded and the supernatant transferred into new tubes, and stored at -80 °C. Protein content was determined using the BCA protein Assay (Thermo Fisher Scientific). Protein extracts (20 µg) were resuspended in Novex Tris-Glycine SDS Sample Buffer (Thermo Fisher Scientific) containing Sample Reducing Agent, heated for 5 min at 85 °C, and separated on precast Novex Tris-Glycine Mini Gels. Proteins were transferred using iBlot™ 2 on a PVDF membrane, which was then blocked in 5% nonfat dry milk (Biorad Laboratories) in T-TBS for 1h at RT. Membranes were then incubated O/N with anti-Phospho-Gsk3β (Ser9 - D85E12) rabbit monoclonal antibody (1:1.000, cat#5558, Cell Signaling), anti-GSK-3β (3D10) mouse monoclonal antibody (1:1.000, cat#9832, Cell Signaling), and anti-GAPDH (6C5) mouse monoclonal antibody (1:500, cat# sc-32233, Santa Cruz Biotechnologies) in T-TBS with 5% BSA. After incubation, membranes were washed three times in T-TBS for 10 min at RT, and incubated for 1h with anti-mouse horseradish peroxidase-conjugated antibodies (1:10.000, cat#115-035-003, Jackson Immunoresearch Laboratories), or anti-rabbit horseradish peroxidase-conjugated antibodies (1:10.000, cat#111-035-003, Jackson Immunoresearch Laboratories) at RT. Reactivity was detected using Western Bright ECL spray device (cat#K-12049-D50, Advansta, Aurogene) and Fluorchem E (ProteinSimple). Densitometric analysis was performed using the ImageJ software (http://rsb.info.nih.gov/ij/).

Calcium imaging

Changes in free intracellular Ca^{2+} concentration $[Ca^{2+}]_i$ were quantified by time-resolved digital fluorescence microscopy using the Ca^{2+} indicator Fura-2 (excitation 340 nm and 380 nm, emission 510 nm). The changes of $[Ca^{2+}]_i$ were expressed as R = F340/F380. iPSCs-derived neuronal cells were incubated with the cell-permeant Fura-2 acetoxylmethylester (2 µM; Molecular probes, Life technologies) for 1 h at 37 °C in culture medium. Ca^{2+} responses were elicited by administering the neurotransmitter or the agonist dissolved in normal external solution for 3 s. Cells were continuously perfused during the experiment. $[Ca^{2+}]_i$ variations were obtained separately from each individual cell, using the MetaFluor 7.0 software (Molecular Devices, USA).

Amplitude values were expressed as means ± S.D. and analyzed using one-way ANOVA test. When necessary, the non-parametric Dunn's one-way ANOVA on ranks was used. In case of significance, all pairwise multiple comparison procedure was used (Holm-Sidak, or Dunn's method for non-parametric tests). Responsive cells data were expressed as % and analyzed using chi-square test. The minimum power of statistical tests was set at 0.8. The significance for all tests was set at $p < 0.05$.

AUTHOR CONTRIBUTION

Conceptualization, M.C.B., M.A.L., V.L.K., S.M., S.F., A.R.; Formal analysis, M.C.B., T.D., A.C., D.S.; Investigation, M.C.B., T.D., D.S.; Methodology, M.C.B., T.D., A.C., M.M., V.d.T., R.R.N., M.R, Z.B., V.A.B., E.A.V., L.B., A.N.B., R.P., D.W.; Resources: I.M.; Project administration, A.R.; Supervision, E.D.B., G.G.T., M.A.L., V.L.K., S.M., S.F., A.R.; Writing—original draft, A.R.; Writing - Review & Editing, M.C.B., T.D., A.C., S.M., S.F., A.R.. All authors read and approved the final manuscript.

ACKNOWLEDGEMENTS

The authors wish to thank the Imaging Facility at Center for Life Nano Science, Fondazione Istituto Italiano di Tecnologia, for support and technical advice. We thank the Genome Engineering & Stem Cell Center (GESC@MGI) at the Washington University in St. Louis for cell line engineering services. We thank Federico Salaris and the other members of the Rosa lab for helpful discussion. We thank Koval Alexey and the other members of the Katanaev lab for support and helpful discussions. We thank Dr. Maryana Bardina for providing patient's fibroblasts. This work was partially supported by "APS Famiglie GNAO1", Sapienza University of Rome, Fondazione Istituto Italiano di Tecnologia

to A.R., by the Russian Science Foundation Grant #21-15-00138 to D.S. and V.L.K., by the Ministry of Science and Higher Education of the Russian Federation grant #075-15-2019-1669 to M.A.L., E.A.V., A.N.B, L.B., and by Istituto Superiore di Sanità (Ricerca Indipendente 2020-2022_ISS20-0ab01a06bd2a) and ISS - Collezione Nazionale di Composti Chimici e Centro di screening (CNCCS) (Rare, Neglected and Poverty Related Diseases – GNAO1 Project) to S.M.

COMPETING INTERESTS

The authors declare no competing interests.

REFERENCES

Akamine, Y., Yasuda, R., Yaguchi, K., Nakamura, Y., Araki, T., & Kamiya, N. (2020). GNAO1 organizes the cytoskeletal remodeling and firing of developing neurons. The FASEB Journal, 34(12), 16601-16621.

Ananth, A. L., Robichaux, M. A., Kim, S., Lindy, A. S., Fleisch, V. C., & Waskiewicz, A. J. (2016). Clinical course of six children with GNAO1 mutations causing a severe and distinctive movement disorder. Pediatric neurology, 59, 81-84.

Bem, J., Zaremba, J., & Dziembowska, M. (2019). Wnt/β-catenin signaling in brain development and mental disorders: keeping TCF7L2 in mind. FEBS Lett, 593, 1654-1674.

Brighi, C., Nardecchia, F., Magri, L., Galli, S., Bonvicini, C., Baroncini, A., & Mingardi, J. (2021). Novel fragile X syndrome 2D and 3D brain models based on human isogenic FMRP-KO iPSCs. Cell Death and Disease, 12, 498.

Chatterjee, P., Gleason, K. W., & Ryan, J. M. (2021). Plasma glial fibrillary acidic protein is elevated in cognitively normal older adults at risk of Alzheimer's disease. Translational psychiatry, 11(1), 27.

Colecraft, H. M., Patil, P. G., & Yue, D. T. (2001). G-protein inhibition of N-and P/Q-type calcium channels: distinctive elementary mechanisms and their functional impact. Journal of Neuroscience, 21(4), 1137-1147.

Conway, J. R., Lex, A., & Gehlenborg, N. (2017). UpSetR: an R package for the visualization of intersecting sets and their properties. Bioinformatics, 33, 2938–2940.

Crespo, M., Smith, D. B., Fletcher, R., Willis, C., & White, P. (2022). Tbr1 Misexpression Alters Neuronal Development in the Cerebral Cortex. Molecular Neurobiology, 59(9), 5750-5765.

Danti, F. R., Galosi, S., Romaniello, R., & Mencarelli, M. A. (2017). GNAO1 encephalopathy: Broadening the phenotype and evaluating treatment and outcome. Neurol Genet, 3, e143.

Darbandi, R., Pacey, L. K., Nakajima, M., Tanaka, K. F., & Hampson, D. R. (2018). Neonatal Tbr1 dosage controls cortical layer 6 connectivity. Neuron, 100(4), 831-845.

Di Rocco, G., Baldassari, S., Borkhardt, A., Drabek, K., Karputkiene, M., Novotna, B., & Carreño, O. (2022). Caenorhabditis elegans provides an efficient drug screening platform for GNAO1-related disorders and highlights the potential role of caffeine in controlling dyskinesia. Human Molecular Genetics, 31, 929–941.

Di Rocco, G. (2023). Phenotypic assessment of pathogenic variants in GNAO1 and response to caffeine in C. elegans models of the disease. Genes, 14(2), 319. doi:10.3390/genes14020319

Dobin, A., Davis, C. A., Schlesinger, F., Drenkow, J., Zaleski, C., Jha, S., Batut, P., Chaisson, M., Gingeras, T. R. (2013). STAR: ultrafast universal RNA-seq aligner. Bioinformatics, 29, 15–21.

Englund, C., Fink, A., Lau, C., Pham, D., Daza, R. A., Bulfone, A., Kowalczyk, T., & Hevner, R. F. (2005). Pax6, Tbr2, and Tbr1 are expressed sequentially by radial glia, intermediate progenitor cells, and postmitotic neurons in developing neocortex. Journal of Neuroscience, 25(1), 247-251.

Fremion, F., Stacey, S., Dagnino-Acosta, A., Dumesnil, V., & Halder, G. (1999). The heterotrimeric protein Go is required for the formation of heart epithelium in Drosophila. Journal of Cell Biology, 145(5), 1063-1076.

Ganne, V., Coulombe, J., Zhang, Y., Daoud, H., Camu, W., Dion, P. A., & Rouleau, G. A. (2022). Glial Fibrillary Acidic Protein: A Biomarker and Drug Target for Alzheimer's Disease. Pharmaceutics, 14(7), 1354.

Gu, Z., Eils, R., & Schlesner, M. (2016). Complex heatmaps reveal patterns and correlations in multidimensional genomic data. Bioinformatics, 32, 2847–2849.

Guillén, I., Gutiérrez, L., Cárcamo, J., & Díaz-Benjumea, F. J. (1991). The transduction signalling protein G0 during embryonic development of Drosophila melanogaster. Cellular Signalling, 3(4), 341-352.

Harrow, J., Frankish, A., Gonzalez, J. M., Tapanari, E., Diekhans, M., Kokocinski, F., ... & Hubbard, T. J. (2012). GENCODE: the reference human genome annotation for The ENCODE Project. Genome Research, 22, 1760–1774.

Jassal, B., Matthews, L., Viteri, G., Gong, C., Lorente, P., Fabregat, A., Sidiropoulos, K., Cook, J., Gillespie, M., Haw, R., Loney, F., May, B., Milacic, M., Rothfels, K., Sevilla, C., Shamovsky, V., Shorser, S., Varusai, T., Weiser, J., Wu, G., Stein, L., Hermjakob, H., & D'Eustachio, P. (2020). The reactome pathway knowledgebase. Nucleic Acids Research, 48, D498-D503.

Jiang, M., Spicher, K., Boulay, G., Wang, Y., Birnbaumer, L., & Rubin, C. S. (1998). Multiple neurological abnormalities in mice deficient in the G protein Go. Proceedings of the National Academy of Sciences, 95(6), 3269–3274. doi:10.1073/pnas.95.6.3269

Katanaev, V. L., Ponzielli, R., Séméria, M., Tomlinson, A. (2005). Trimeric G protein-dependent frizzled signaling in Drosophila. Cell, 120, 111–122.

Kim, W. Y., Wang, X., Wu, Y., Doble, B. W., Patel, S., Woodgett, J. R., & Snider, W. D. (2011). GSK3 signaling in neuronal development. Frontiers in Molecular Neuroscience, 4, 48.

Knight, A., Cao, Y., Gohlke, M., & Kim, S. (2021). A universal allosteric mechanism for G protein activation. Molecular Cell, 81, 1384–1396.e6.

Koval, A., Katanaev, V. L. (2011). Wnt3a stimulation elicits G-protein-coupled receptor properties of mammalian Frizzled proteins. Biochem J, 433, 435–440.

Krenn, M., Hess, E., & Blau, N. (2022). GNAO1 Haploinsufficiency Associated with a Mild Delayed-Onset Dystonia Phenotype. Movement Disorders, 37, 2464-2466. doi: 10.1002/mds.29258.

Langmead, B., & Salzberg, S. (2012). Fast gapped-read alignment with Bowtie 2. Nature Methods, 9, 357–359.

Larasati, A., Dwianingsih, E. K., & Sugandha, I. K. (2022). Restoration of the GTPase activity and cellular interactions of Gαo mutants by Zn2+ in GNAO1 encephalopathy models. Science Advances, 8(40), eabn9350.

Larrivee, T. M., DiFrancesco, D. C., & Davis, R. L. (2020). Mice with GNAO1 R209H Movement Disorder Variant Display Hyperlocomotion Alleviated by Risperidone. Journal of Pharmacology and Experimental Therapeutics, 373, 24–33.

Liao, Y., Smyth, G. K., & Shi, W. (2019). WebGestalt 2019: Gene set analysis toolkit with revamped UIs and APIs. Nucleic Acids Research, 47, W199–W205.

Love, M. I., Huber, W., & Anders, S. (2014). Moderated estimation of fold change and dispersion for RNA-seq data with DESeq2. Genome Biology, 15, 550.

Lunev, E. A., Shmidt, A. A., Vassilieva, S. G., Savchenko, I. M., Loginov, V. A., Marina, V. I., Egorova, T. V., and Bardina, M. V. (2022). Effective Viral Delivery of Genetic Constructs to Neuronal Culture for Modeling and Gene Therapy of GNAO1 Encephalopathy. Molecular Biology 56, 559-571.

McDavid, S., Glajch, K. E., & Eberwine, J. H. (2006). G-proteins modulate cumulative inactivation of N-type (Cav2.2) calcium channels. Journal of Neuroscience, 26(51), 13373-13383.

Muntean, B. S., Zucca, S., & Assis-Nascimento, P. (2021). Gαo is a major determinant of cAMP signaling in the pathophysiology of movement disorders. Cell Reports, 34(5), 108718.

Nakamura, Y., Okamoto, N., & Nakamura, K. (2013). De Novo mutations in GNAO1, encoding a Gαo subunit of heterotrimeric G proteins, cause epileptic encephalopathy. The American Journal of Human Genetics, 93(3), 496-505.

Pacey, L. K., Doss, L., & Gourley, S. L. (2015). Persistent astrocyte activation in the fragile X mouse cerebellum. Brain and Behavior, 5(10), e00400.

Saitsu, H., Akita, T., & Tohyama, J. (2016). Phenotypic spectrum of GNAO1 variants: epileptic encephalopathy to involuntary movements with severe developmental delay. European Journal of Human Genetics, 24, 129–134.

Sandoe, J., & Eggan, K. (2013). Opportunities and challenges of pluripotent stem cell neurodegenerative disease models. Nature Neuroscience, 16, 780–789.

Savitsky, P., Kadir, R., & Sprecher, S. G. (2020). Humanization of Drosophila Gαo to Model GNAO1 Paediatric Encephalopathies. Biomedicines, 8(10).

Silachev, D. N., Usatikova, E. A., & Pevzner, I. B. (2022). Mouse models characterize GNAO1 encephalopathy as a neurodevelopmental disorder leading to motor anomalies: from a severe G203R to a milder C215Y mutation. Acta Neuropathologica Communications, 10(1), 1-17.

Soldner, F., Laganière, J., Cheng, A. W., Hockemeyer, D., Gao, Q., Alagappan, R., Khurana, V., Golbe, L. I., Myers, R. H., Lindquist, S., et al. (2011). Generation of isogenic pluripotent stem cells differing exclusively at two early onset Parkinson point mutations. Cell, 146, 1358–1367.

Sunamura, N., Akiyama, M., & Honda, Y. (2018). Loss of the fragile X mental retardation protein causes aberrant differentiation in human neural progenitor cells. Scientific Reports, 8(1), 11585.

Vasques, J. F., Mendez-Otero, R., & Gubert, F. (2020). Modeling ALS using iPSCs: Is it possible to reproduce the phenotypic variations observed in patients in vitro? Regenerative Medicine. https://doi.org/10.2217/rme-2020-0067

Vigont, V.A., Grekhnev, D.A., Lebedeva, O.S., Gusev, K.O., Volovikov, E.A., Skopin, A.Y., Bogomazova, A.N., Shuvalova, L.D., Zubkova, O.A., Khomyakova, E.A., et al. (2021). STIM2 Mediates Excessive Store-Operated Calcium Entry in Patient-Specific iPSC-Derived Neurons Modeling a Juvenile Form of Huntington's Disease. Front Cell Dev Biol 9, 625231.

Wang, X., Chen, Y., & Zhang, Y. (2022). Genetic modeling of GNAO1 disorder delineates mechanisms of Gαo dysfunction. Human Molecular Genetics, 31(4), 510-522.

Wettschureck, N., & Offermanns, S. (2005). Mammalian G proteins and their cell type specific functions. Physiological Reviews, 85, 1159–1204.

Whye, D., Wood, D., Saber, W. A., Norabuena, E. M., Makhortova, N. R., Sahin, M., Buttermore, E. D. (2023). A Robust Pipeline for the Multi-Stage Accelerated Differentiation of Functional 3D Cortical Organoids from Human Pluripotent Stem Cells. Curr Protoc, 3, e641.

Wirth, T., Blau, N., & Klopstock, T. (2022). Highlighting the Dystonic Phenotype Related to GNAO1. Movement Disorders, 37, 1547-1554. doi: 10.1002/mds.29074.

Wolfgang, W. J., Quan, F., & Wright, R. J. (1991). Restricted spatial and temporal expression of G-protein alpha subunits during Drosophila embryogenesis. Development, 113(2), 527-538.

Wong, N. C., Chung, S. K., & Tidball, A. M. (2019). FOXG1-related syndrome: from clinical to molecular genetics and pathogenic mechanisms. International Journal of Molecular Sciences, 20(17), 4176.

Worley, P. F., Baraban, J. M., & Snyder, S. H. (1986). Go, a guanine nucleotide-binding protein: immunohistochemical localization in rat brain resembles distribution of second messenger systems. Proceedings of the National Academy of Sciences, 83(12), 4561-4565.

Zamponi, G. W., Bourinet, E., & Nelson, D. (2013). Regulation of CaV2 calcium channels by G protein-coupled receptors. Biochimica et Biophysica Acta (BBA)-Biomembranes, 1828(7), 1629-1643.

Zhu, A., Ibrahim, J. G., & Love, M. I. (2019). Heavy-tailed prior distributions for sequence count data: removing the noise and preserving large differences. Bioinformatics, 35, 2084–2092.

FIGURE LEGENDS

Figure 1. RNA-Seq analysis of neural progenitors

A. Outline of the origin of the hiPSC lines used in this study. **B.** Heatmap showing the expression in GNAO1$^{+/G203R}$ and GNAO1$^{+/G203G}$ NPCs at day 7 and 11 of the leading edge genes identified via GSEA for the "cell fate commitment" Gene Ontology Biological Process category. Genes that were identified as leading edge ones only at day 7, only at day 11, or at both time points were split into three groups (Only_D7, Only D11, Common_D7-D11, respectively). Genes belonging to the "neuron fate commitment" or "neuron fate specification" categories were colored in purple. **C.** Heatmap showing the expression in GNAO1$^{+/G203R}$ and GNAO1$^{+/G203G}$ NPCs at day 7 and 11 of selected neuron progenitor- and reactive astrocyte-specific genes. The adjusted p-values displayed on the right pertain to the DGE analyses performed between GNAO1$^{+/G203R}$ and GNAO1$^{+/G203G}$ NPCs at day 7 (FDR D7) and day 11 (FDR D11). The expression values reported in both heatmaps correspond to row-scaled (Z-score), rlog-transformed count data.

Figure 2. Cortical neuron differentiation and analysis at day 25.

A. Schematic representation of the protocol used for cortical neuron differentiation of human iPSCs in conventional 2D cultures. NPC: neural progenitor cell; SB: SB431542 (TGFβ type I receptor/ALK5 inhibitor); LDN: LDN193189 (BMP inhibitor); DAPT: Notch inhibitor; BDNF: Brain Derived Neurotrophic Factor; GDNF: Glial Derived Neurotrophic Factor; AA: ascorbic acid; cAMP: cyclic AMP. **B.** Phase contrast images of differentiating cells at day 25. **C.** Real-time qRT-PCR analysis of the expression of the indicated markers in differentiating cells. The graphs show the average and standard deviation (Student's t test; paired; two tails; **$p<0.01$, ***$p<0.001$).

Figure 3. Immunostaining analysis at day 25 of differentiation

Immunostaining analysis with the indicated primary antibodies and DAPI to label nuclei. PAX6 and NESTIN are neural progenitor markers; TBR2 is a neuronal precursor marker; TUJ1 and MAP2 are neuronal markers.

Figure 4. Analysis of neuronal rosettes morphology in the independent GNAO1$^{+/G203R}$#2 line

A. Phase contrast images of GNAO1$^{+/G203R}$#2 cells at the neural rosette stage, corresponding to day 30 of differentiation. Note that the in the protocol used for differentiation of GNAO1$^{+/G203R}$#2 cells (as described in the Methods section) has a different timing from the one depicted in figure 2A. **B-D**. Immunostaining was performed using the specified primary antibodies along with DAPI for nuclear labeling. TBR1 is a marker of early-born neurons (B); and TUJ1 (B) and MAP2 (C) are markers for neurons; NESTIN serves as a marker for neural progenitors (C); β-catenin as a marker of apical polarization in neural rosettes (D). Number of individual cultures for experiments was 3.

Figure 5. Marker expression analysis at day 40 of differentiation

A. Real-time qRT-PCR analysis of the expression of the indicated markers in differentiating cells. The graphs show the average and standard deviation (Student's t test; paired; two tails; *p<0.05, ***p<0.001, n.s. nonsignificant). **B.** Immunostaining analysis with the indicated primary antibodies and DAPI to label nuclei.

Figure 6. Marker expression analysis at day 50 and 70 of differentiation

A-B. Real-time qRT-PCR analysis of the expression of the indicated markers in differentiating cells at the indicated time points. The graphs show the average and standard deviation (Student's t test; paired; two tails; *p<0.05, ***p<0.001, n.s. nonsignificant). **C.** Immunostaining analysis with the indicated primary antibodies and DAPI to label nuclei.

Figure 7. Neurons carrying the p.G203R GNAO1 substitution exhibit lower values of basal $[Ca^{2+}]_i$ and a reduced spontaneous Ca^{2+} activity.

A. representative spontaneous Ca^{2+} transients recorded in control cells. **B.** up, $[Ca^{2+}]_i$ basal values measured in individual cells. Please note the reduced basal $[Ca^{2+}]_i$ for p.G203R mutant neurons. Number of examined cells: 160, 159, 229 and 230, for p.G203G DIV40, p.G203R DIV40, p.G203G DIV50 and p.G203R DIV50, respectively. Bottom, percentage of neurons exhibiting spontaneous Ca^{2+} transients, same cells as upper panel. *, p<0.001.

Figure 8. The p.G203R GNAO1 substitution reduces the response of differentiated neurons to several neurotransmitters in terms of $[Ca^{2+}]_i$ elevations.

A. left, percentage of neurons exhibiting Ca^{2+} transients induced by the application of glutamate (1 mM, 3 s); inset, representative Ca^{2+} transients elicited by glutamate administration (1 mM, 3 s), in a control (black) and p.G203R GNAO1 mutated (red) iPSC-derived neuronal cells. Number of examined cells: 160, 159, 229 and 230, for p.G203G DIV40, p.G203R DIV40, p.G203G DIV50 and p.G203R DIV50, respectively. Right, amplitude of the $[Ca^{2+}]_i$ increase induced by glutamate application in the responding cells. **B.** left, percentage of neurons exhibiting Ca^{2+} transients induced by the application of GABA (100 μM, 3 s). Same cells as fig. 7A. Right, amplitude of the $[Ca^{2+}]_i$ increase induced by GABA application in the responding cells. **C.** left, percentage of neurons exhibiting Ca^{2+} transients induced by the application of baclofen (100 μM, 3 s). Same cells as fig. 7A. Right, amplitude of the $[Ca^{2+}]_i$ increase induced by baclofen application in the responding cells. **D.** left, percentage of neurons exhibiting Ca^{2+} transients induced by the application of glycine (30 μM, 3 s). Same cells as fig. 7A. Right, amplitude of the $[Ca^{2+}]_i$ increase induced by glycine application in the responding cells. **E.** left, percentage of neurons exhibiting Ca^{2+} transients induced by the application of ACh (100 μM, 3 s). Same cells as fig. 7A. Right, amplitude of the $[Ca^{2+}]_i$ increase induced by ACh application in the responding cells. **F**. left, percentage of neurons exhibiting Ca^{2+} transients induced by the application of ATP (100 μM, 3 s). Same cells as fig. 7A. Right, amplitude of the $[Ca^{2+}]_i$ increase induced by ATP application in the responding cells. *, $p<0.001$; a, $p=0.008$; b, $p=0.022$; c, $p=0.006$, d, $p=0.007$.

Supplementary Figure S1. RNA-Seq analysis: PCA and UpSet plot

A. PCA plot of RNA-Seq data from GNAO1$^{+/G203R}$ and GNAO1$^{+/G203G}$ NPCs at day 7 and 11. **B.** UpSet plot showing the overlap of genes that are differentially expressed between GNAO1$^{+/G203R}$ and GNAO1$^{+/G203G}$ NPCs (adjusted *p*-value < 0.01) at the two time points.

Supplementary Figure S2. GSEA results

A-C. Barplots showing the results of the GSEAs performed on the GNAO1$^{+/G203R}$ vs GNAO1$^{+/G203G}$ contrast at day 7 and day 11. Only categories with absolute Normalized Enrichment Score (NES) > 1.7 and FDR-adjusted p-value < 0.05 in at least one time point are reported. Functional categories are indicated above each panel. The Gene Ontology (GO) terms correspond to the non-redundant sets provided by WebGestalt. A positive or negative NES indicates that the gene set is enriched among the upregulated or the downregulated genes, respectively. **D.** Heatmap showing the expression in GNAO1$^{+/G203R}$ and GNAO1$^{+/G203G}$ NPCs at day 7 and 11 of the leading edge genes identified via GSEA for the "WNT ligand biogenesis and trafficking" Reactome pathway. Genes that were identified as leading edge ones only at day 7, only at day 11, or at both time points were split into three groups (Only_D7, Only D11, Common_D7-D11, respectively). The reported expression values correspond to row-scaled (Z-score), rlog-transformed count data.

Supplementary Figure S3. Phospho-GSK3β levels at days 40 and 50 of differentiation

Left panel, representative western blot analysis showing levels of phospho-Gsk3β, Gsk3β and GAPDH in differentiating GNAO1-G203R neurons and control isogenic cells (isogenic CTR), at day 40 and 50. Right panel, dot plot shows the quantification of Gsk3β phosphorylation levels in control and p.G203R neurons at day 40 and 50. Graphs indicate the % of phosphoproteins normalized to GAPDH, indicating the total amount of phosphorylated protein inside the cells. Average values and standard deviation are also shown (two tails paired Student's t test; ***p<0.001).

Supplementary Table S1. **Results of the differential expression analyses performed between GNAO1+/G203R and GNAO1+/G203G NPCs at day 7 and day 11**

Primer name	Primer sequence 5'-3'
ATP5O FW	ACTCGGGTTTGACCTACAGC
ATP5O RV	GGTACTGAAGCATCGCACCT
FOXG1 FW	AGGAGGGCGAGAAGAAGAAC
FOXG1 RV	TCACGAAGCACTTGTTGAGG
NESTIN FW	GCGTTGGAACAGAGGTTGGA
NESTIN RV	TGGGAGCAAAGATCCAAGAC
GFAP FW	GATCAACTCACCGCCAACAG
GFAP RV	ATAGGCAGCCAGGTTGTTCT
PAX6 FW	ATGTGTGAGTAAAATTCTGGGCA
PAX6 RV	GCTTACAACTTCTGGAGTCGCTA
TBR2 FW	CTTCTTCCCGGAGCCCTTTGTC
TBR2 RV	TTCGCTCTGTTGGGGTGAAAGG
TBR1 FW	CAACGGAGCCTACAACAGCCTC
TBR1 RV	TGGTAGAACGGAGCTCCTTGGT
OTX2 FW	CAAAGTGAGACCTGCCAAAAAGA
OTX2 RV	TGGACAAGGGATCTGACAGTG

Supplementary Table S2. Sequences of the primers used in this study

A

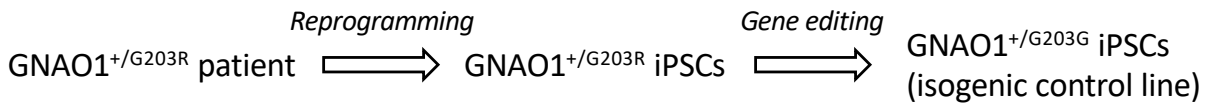
Reprogramming
Gene editing
GNAO1+/G203R patient
GNAO1+/G203R iPSCs
GNAO1+/G203G iPSCs
(isogenic control line)

B

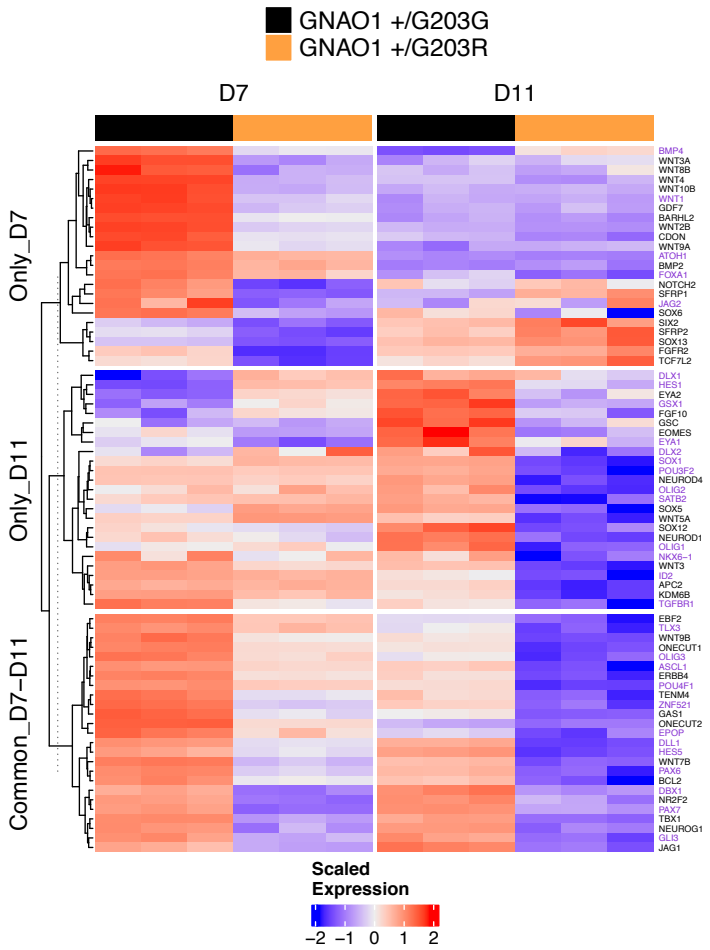
GNAO1 +/G203G
GNAO1 +/G203R
D7
D11
Only_D7
Only_D11
Common_D7–D11
Scaled Expression
−2 −1 0 1 2

C

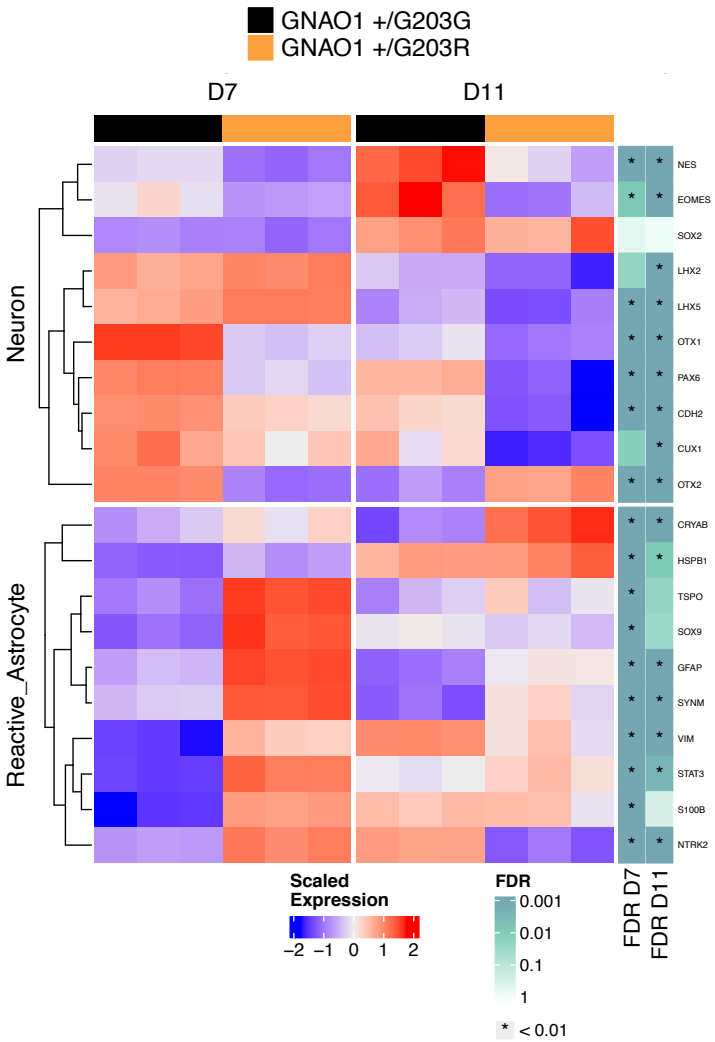
GNAO1 +/G203G
GNAO1 +/G203R
D7
D11
Neuron
Reactive_Astrocyte
NES
EOMES
SOX2
LHX2
LHX5
OTX1
PAX6
CDH2
CUX1
OTX2
CRYAB
HSPB1
TSPO
SOX9
GFAP
SYNM
VIM
STAT3
S100B
NTRK2
Scaled Expression
−2 −1 0 1 2
FDR
0.001
0.01
0.1
1
* < 0.01
FDR D7
FDR D11

A

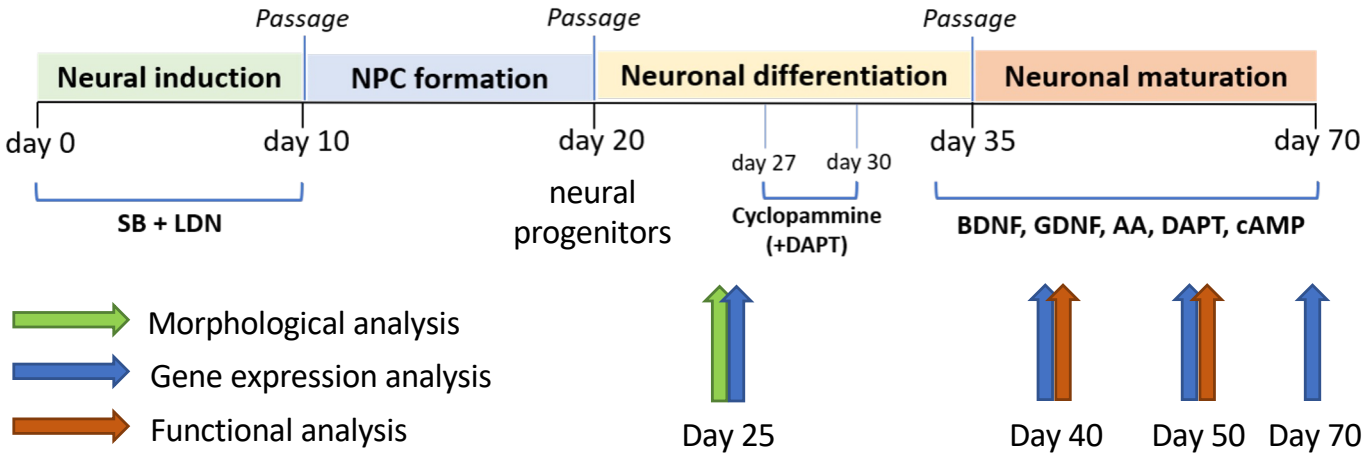

B

GNAO1$^{+/G203G}$

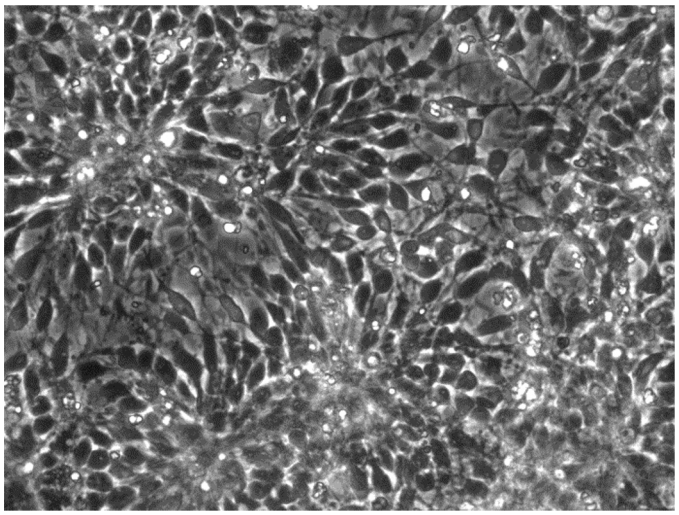

GNAO1$^{+/G203R}$

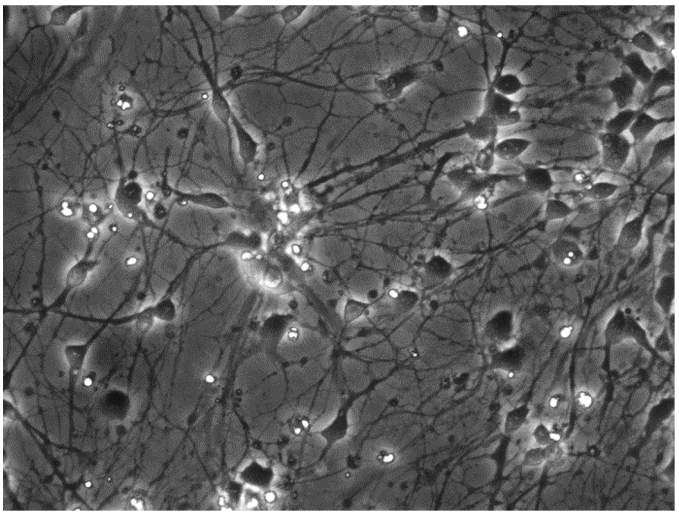

Day 25; n=4

C

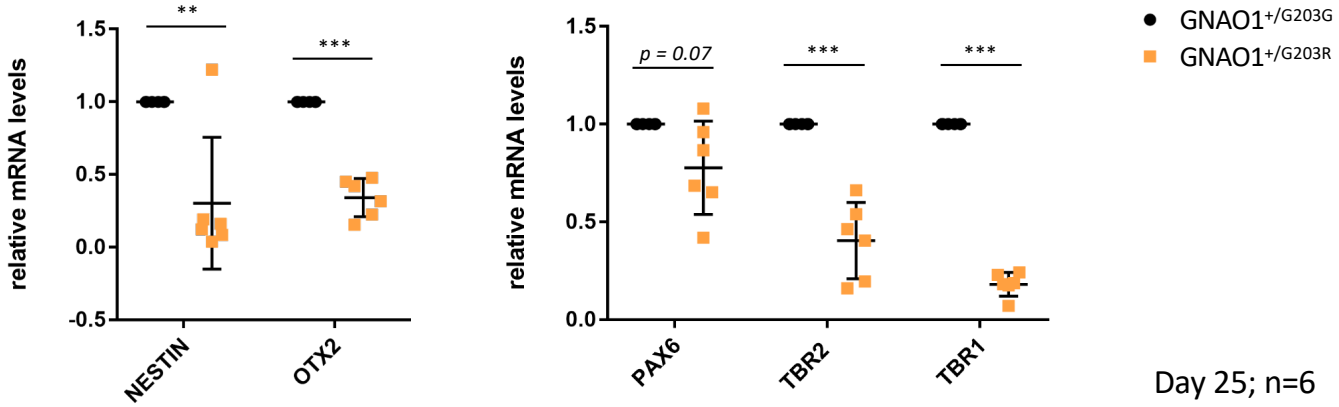

Day 25; n=6

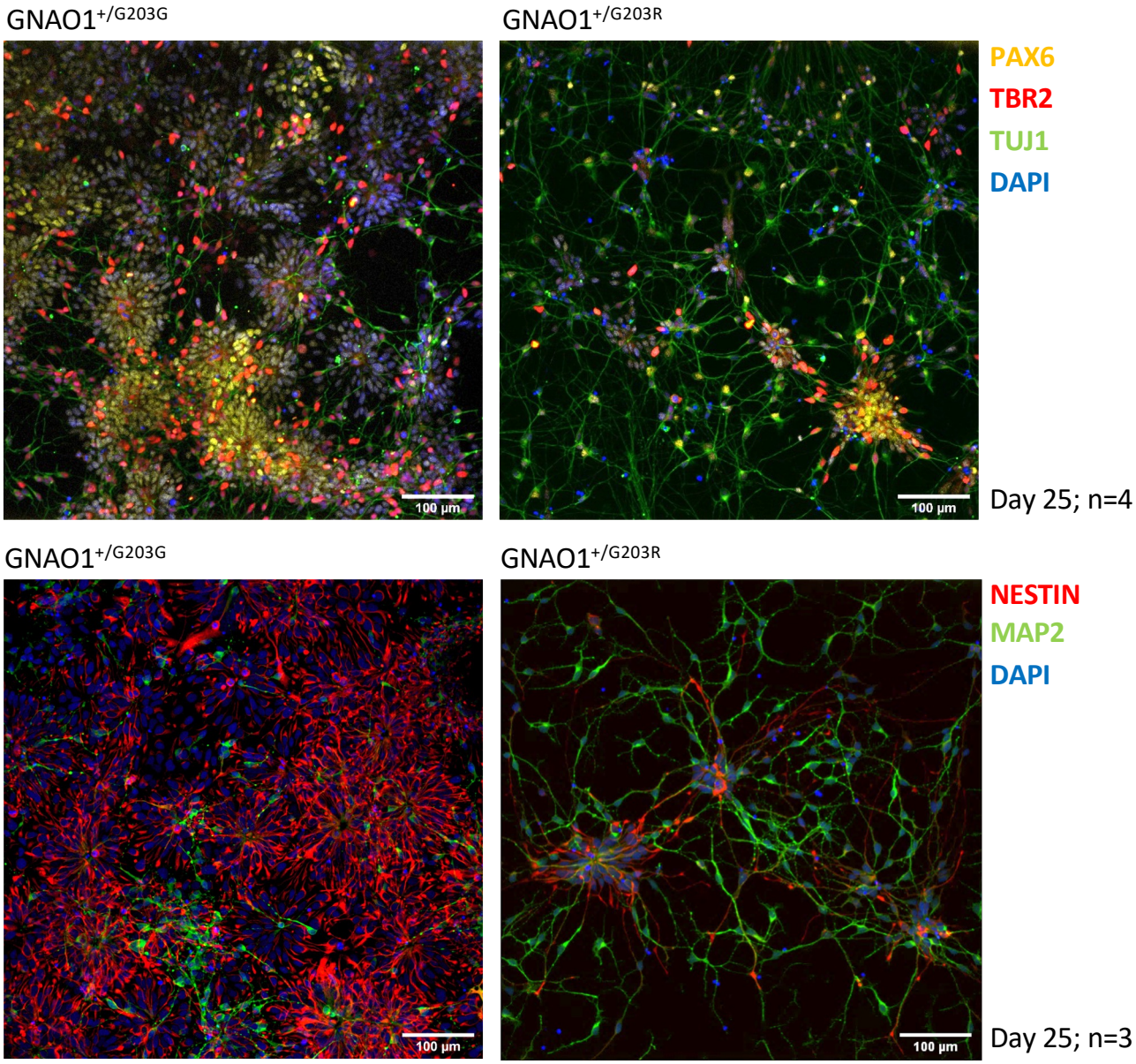
GNAO1+/G203G
GNAO1+/G203R
PAX6
TBR2
TUJ1
DAPI
100 µm
100 µm
Day 25; n=4
GNAO1+/G203G
GNAO1+/G203R
NESTIN
MAP2
DAPI
100 µm
100 µm
Day 25; n=3

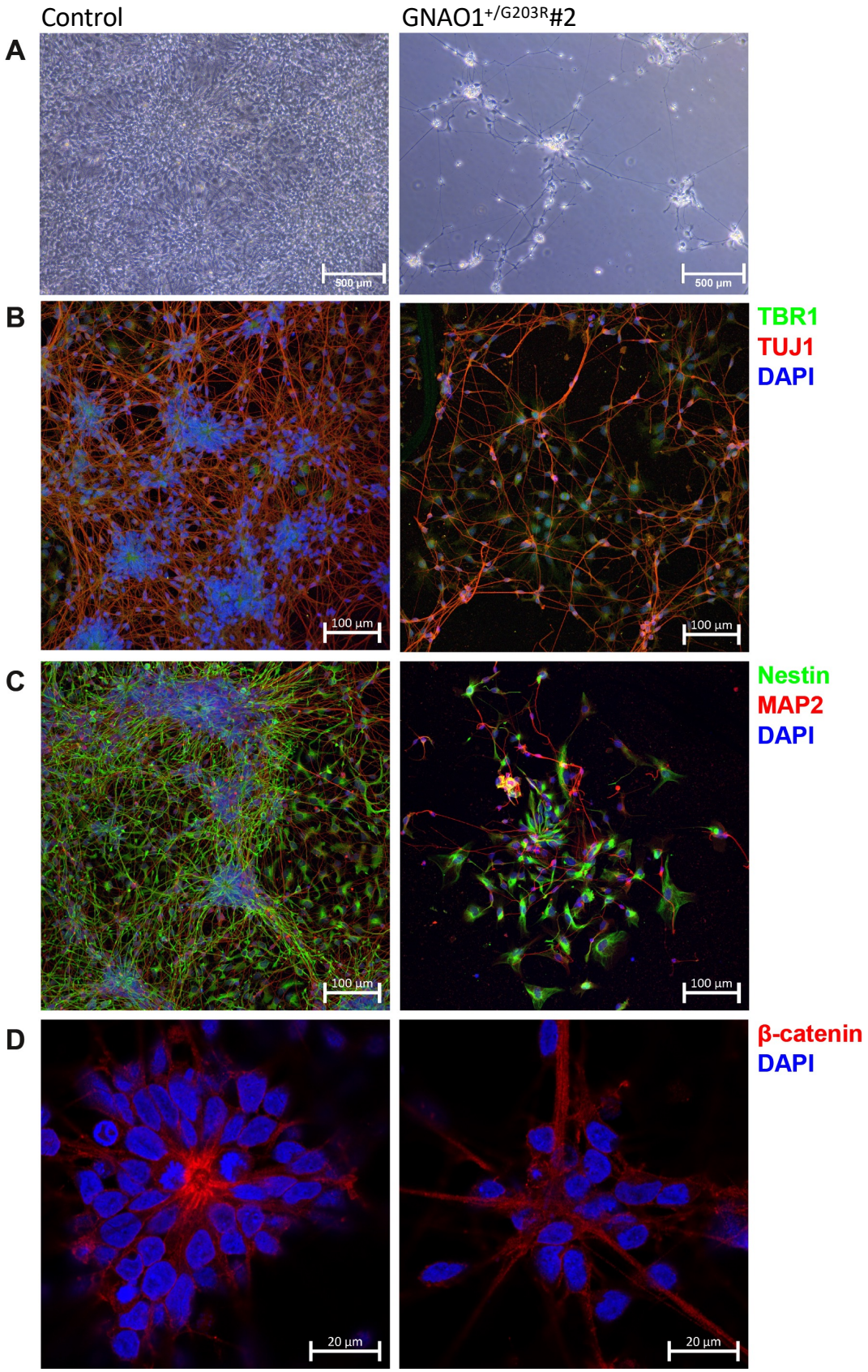
Control
GNAO1+/G203R#2
A
500 µm
500 µm
B
TBR1
TUJ1
DAPI
100 µm
100 µm
C
Nestin
MAP2
DAPI
100 µm
100 µm
D
β-catenin
DAPI
20 µm
20 µm

A

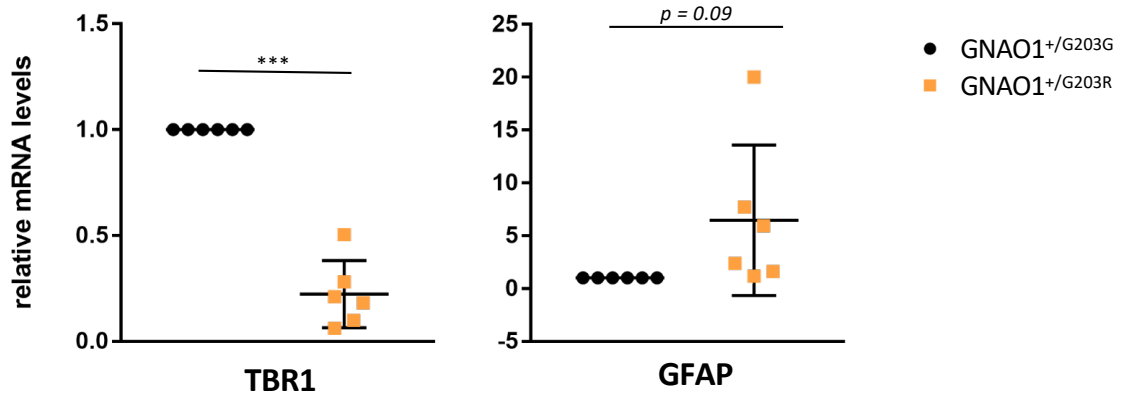

Day 40; n=6 Day 40; n=6

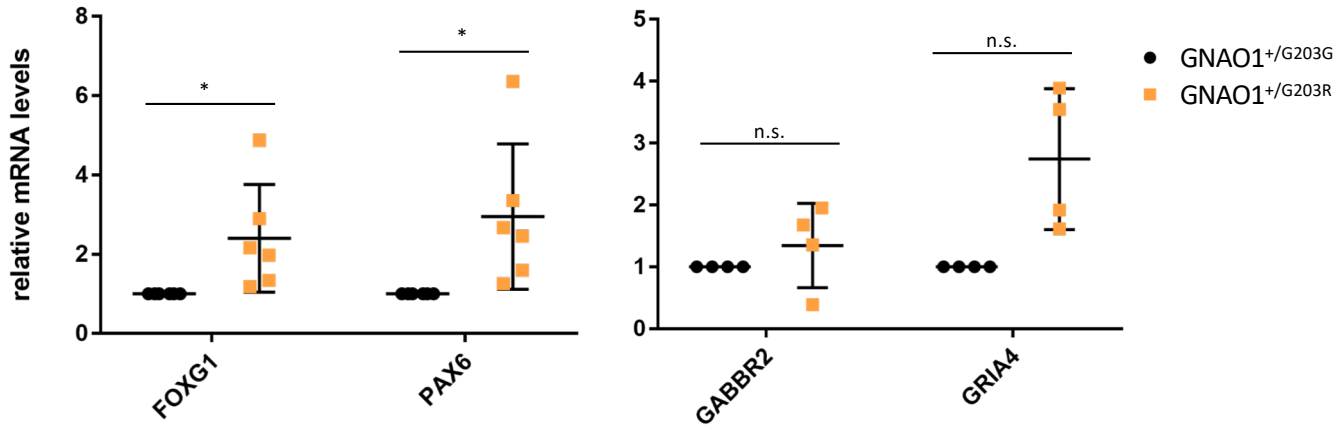

Day 40; n=6 Day 40; n=4

B

GNAO1+/G203G GNAO1+/G203R

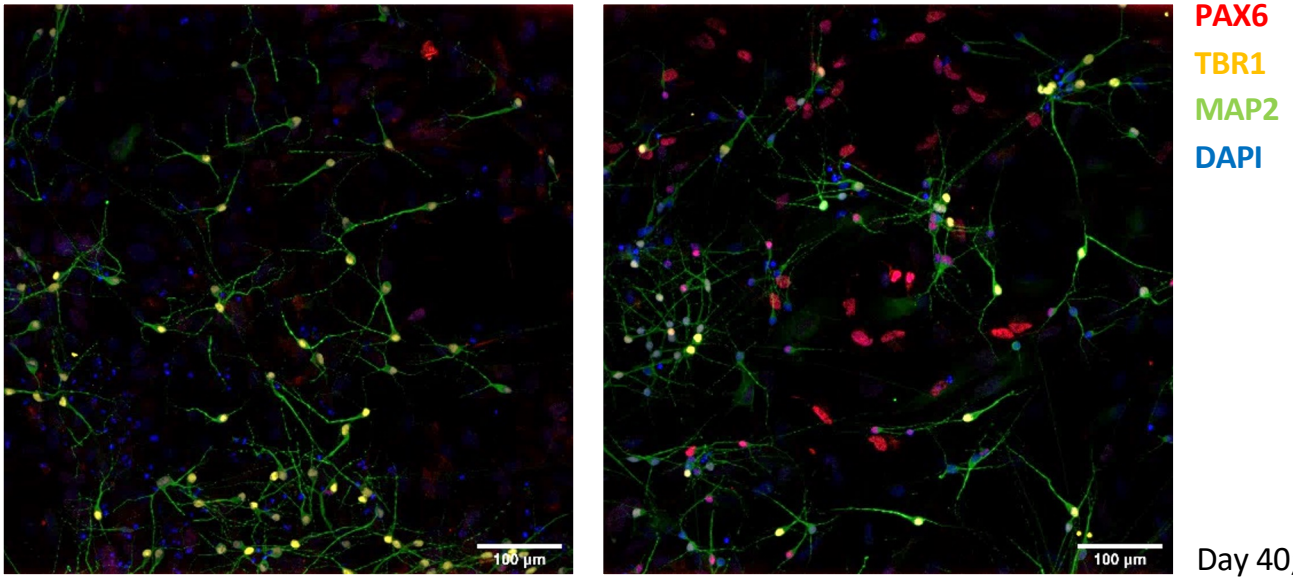

Day 40; n=3

A

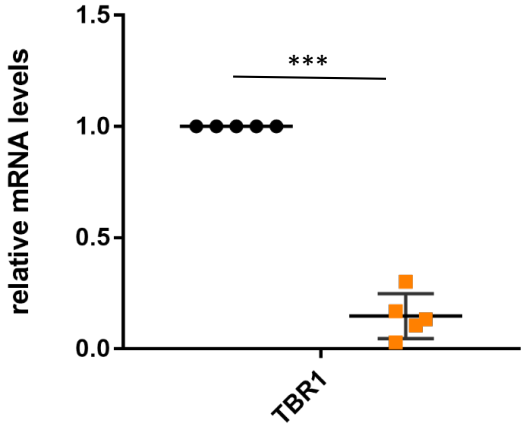

Day 50; n=5

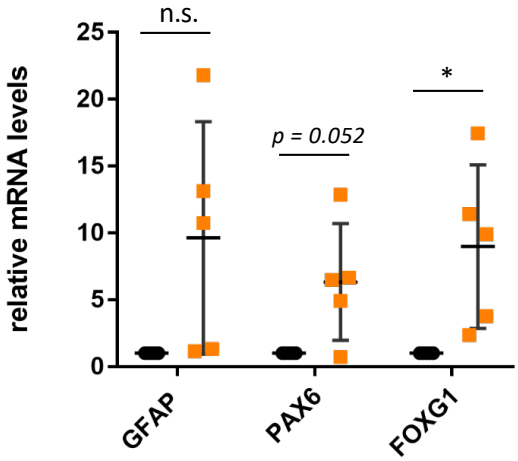

Day 50; n=5

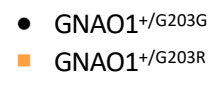

B

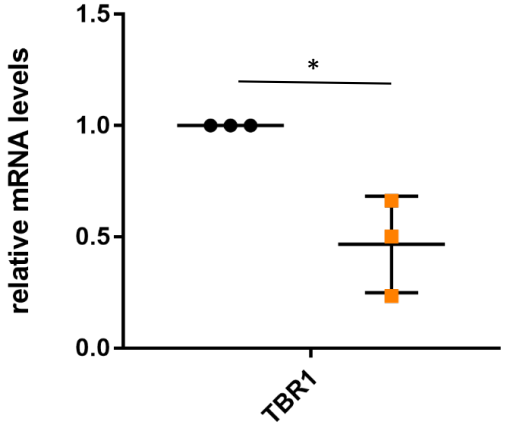

Day 70; n=3

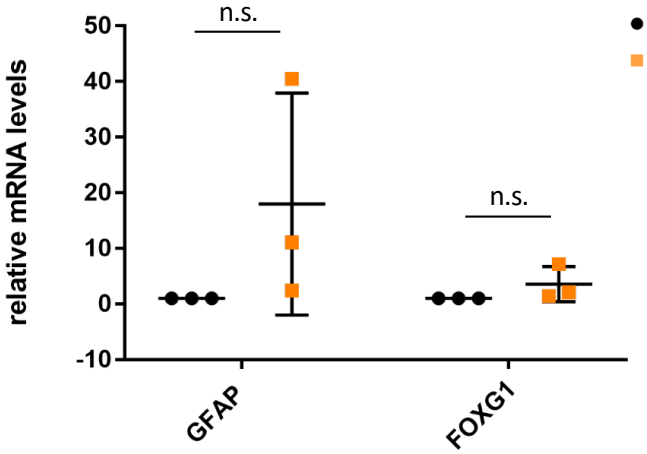

Day 70; n=3

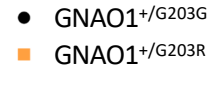

C

GNAO1+/G203G

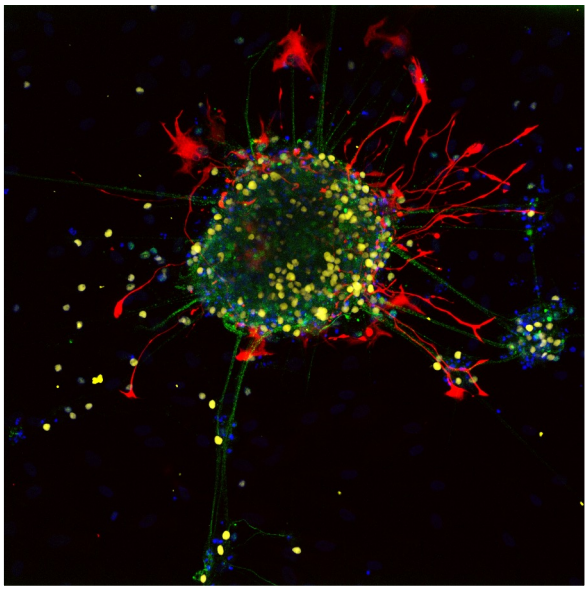

GNAO1+/G203R

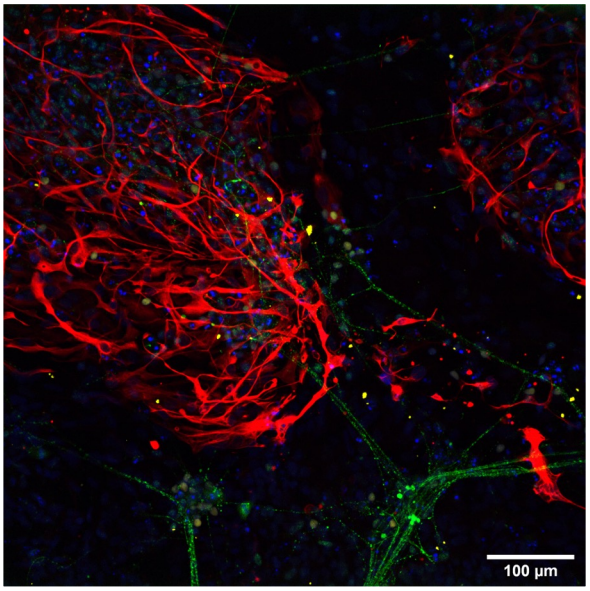

GFAP
TBR1
NF-H
DAPI

Day 50; n=2

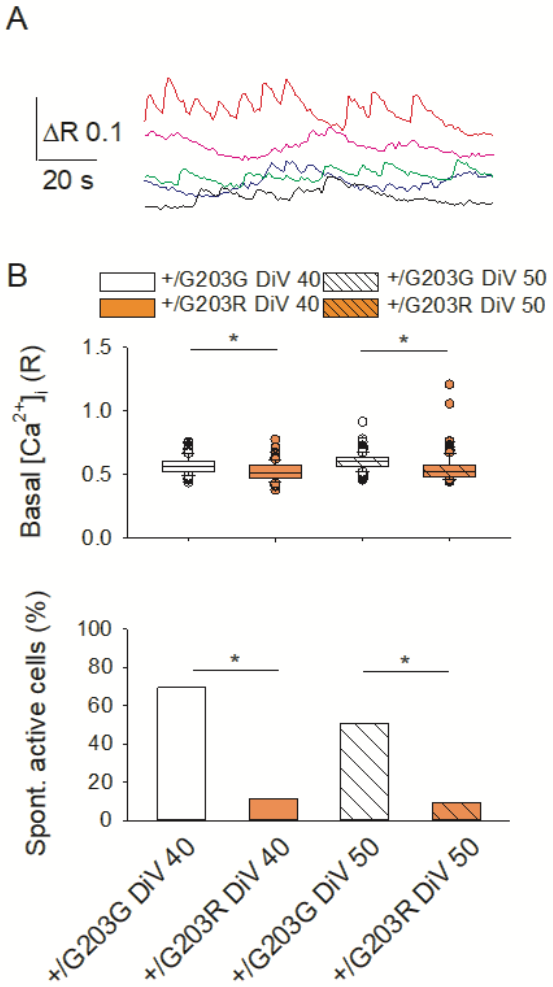
A
ΔR 0.1
20 s
B
+/G203G DiV 40
+/G203G DiV 50
+/G203R DiV 40
+/G203R DiV 50
Basal [Ca2+]i (R)
1.5
1.0
0.5
0.0
*
*
Spont. active cells (%)
100
80
60
40
20
0
*
*
+/G203G DiV 40
+/G203R DiV 40
+/G203G DiV 50
+/G203R DiV 50

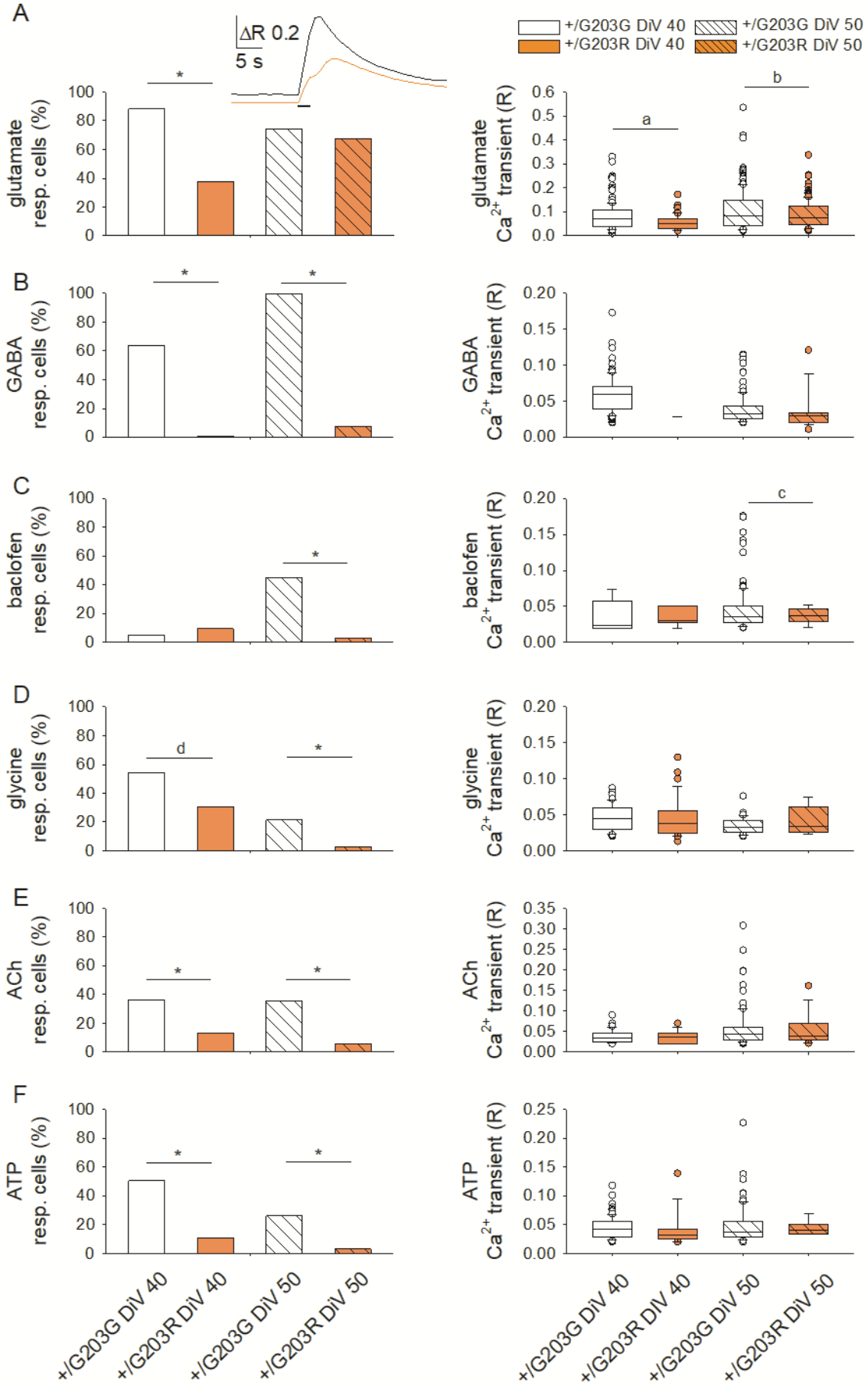
A
ΔR 0.2
5 s
+/G203G DiV 40
+/G203R DiV 40
+/G203G DiV 50
+/G203R DiV 50
glutamate resp. cells (%)
glutamate Ca2+ transient (R)
B
GABA resp. cells (%)
GABA Ca2+ transient (R)
C
baclofen resp. cells (%)
baclofen Ca2+ transient (R)
D
glycine resp. cells (%)
glycine Ca2+ transient (R)
E
ACh resp. cells (%)
ACh Ca2+ transient (R)
F
ATP resp. cells (%)
ATP Ca2+ transient (R)
+/G203G DiV 40
+/G203R DiV 40
+/G203G DiV 50
+/G203R DiV 50

A

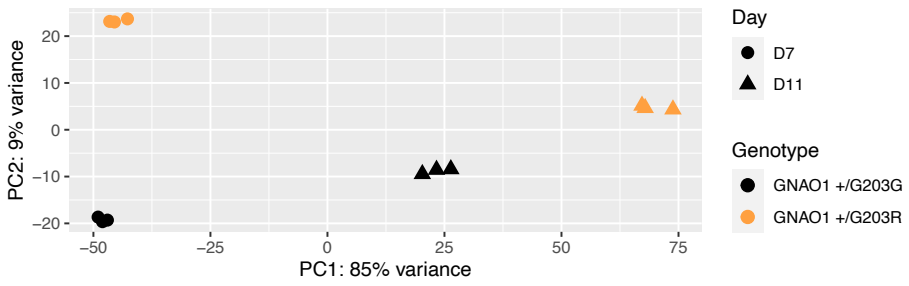
PC2: 9% variance
PC1: 85% variance
20
10
0
−10
−20
−50
−25
0
25
50
75
Day
D7
D11
Genotype
GNAO1 +/G203G
GNAO1 +/G203R

B

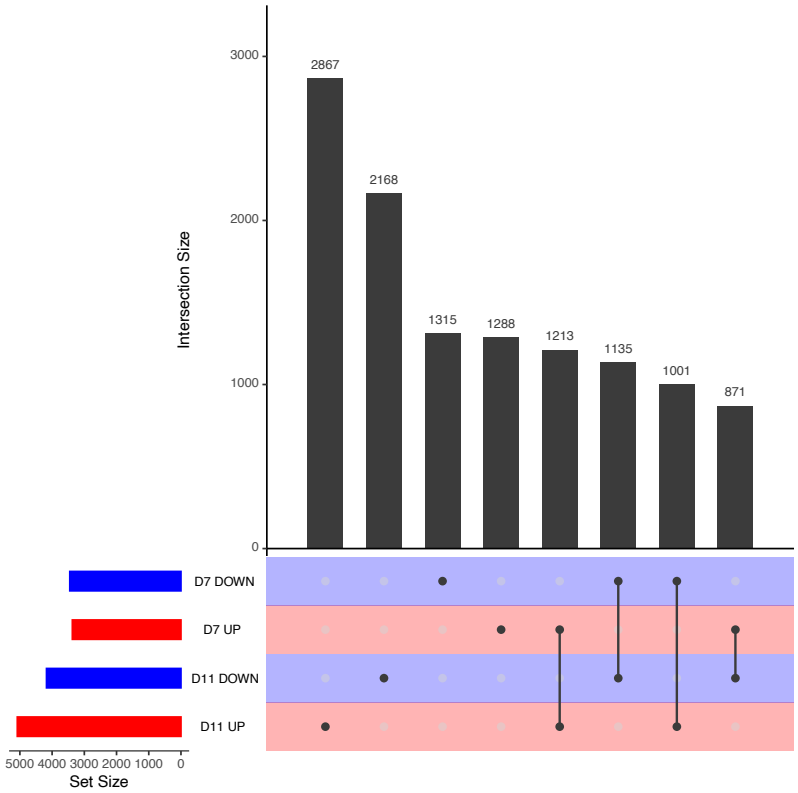
Intersection Size
3000
2000
1000
0
2867
2168
1315
1288
1213
1135
1001
871
D7 DOWN
D7 UP
D11 DOWN
D11 UP
5000 4000 3000 2000 1000 0
Set Size

A

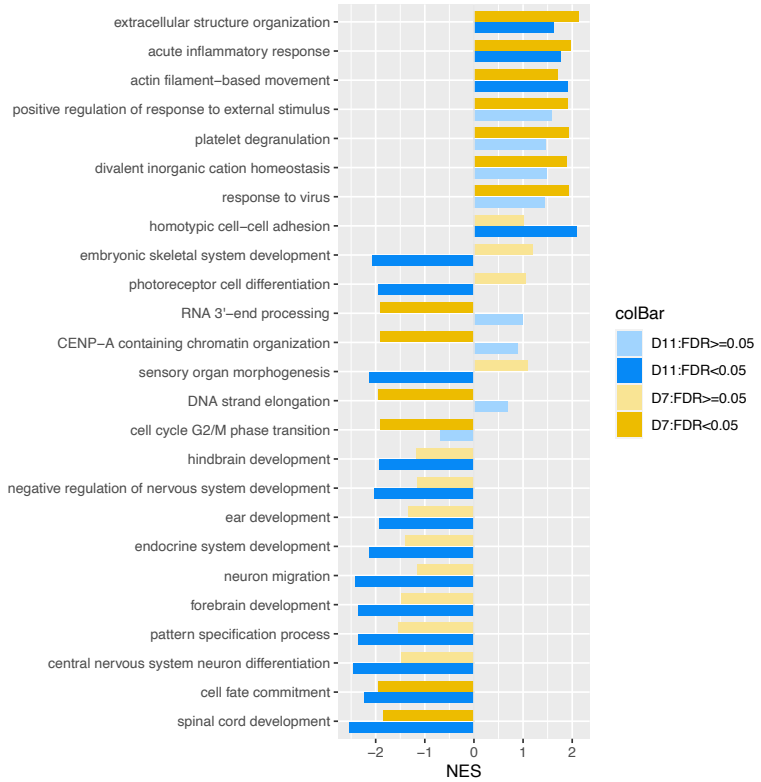
GSEA: biological process
extracellular structure organization
acute inflammatory response
actin filament−based movement
positive regulation of response to external stimulus
platelet degranulation
divalent inorganic cation homeostasis
response to virus
homotypic cell−cell adhesion
embryonic skeletal system development
photoreceptor cell differentiation
RNA 3'−end processing
CENP−A containing chromatin organization
sensory organ morphogenesis
DNA strand elongation
cell cycle G2/M phase transition
hindbrain development
negative regulation of nervous system development
ear development
endocrine system development
neuron migration
forebrain development
pattern specification process
central nervous system neuron differentiation
cell fate commitment
spinal cord development
−2 −1 0 1 2
NES
colBar
D11:FDR>=0.05
D11:FDR<0.05
D7:FDR>=0.05
D7:FDR<0.05

B

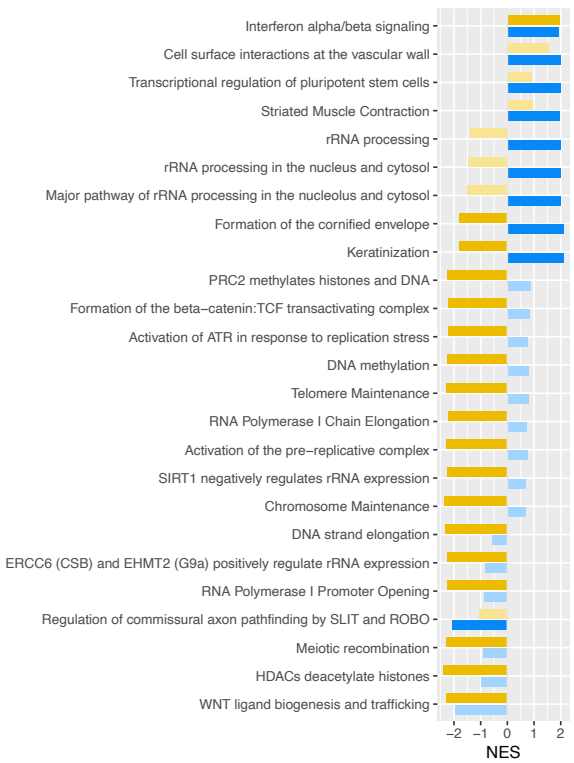
GSEA: reactome
Interferon alpha/beta signaling
Cell surface interactions at the vascular wall
Transcriptional regulation of pluripotent stem cells
Striated Muscle Contraction
rRNA processing
rRNA processing in the nucleus and cytosol
Major pathway of rRNA processing in the nucleolus and cytosol
Formation of the cornified envelope
Keratinization
PRC2 methylates histones and DNA
Formation of the beta−catenin:TCF transactivating complex
Activation of ATR in response to replication stress
DNA methylation
Telomere Maintenance
RNA Polymerase I Chain Elongation
Activation of the pre−replicative complex
SIRT1 negatively regulates rRNA expression
Chromosome Maintenance
DNA strand elongation
ERCC6 (CSB) and EHMT2 (G9a) positively regulate rRNA expression
RNA Polymerase I Promoter Opening
Regulation of commissural axon pathfinding by SLIT and ROBO
Meiotic recombination
HDACs deacetylate histones
WNT ligand biogenesis and trafficking
−2 −1 0 1 2
NES

C

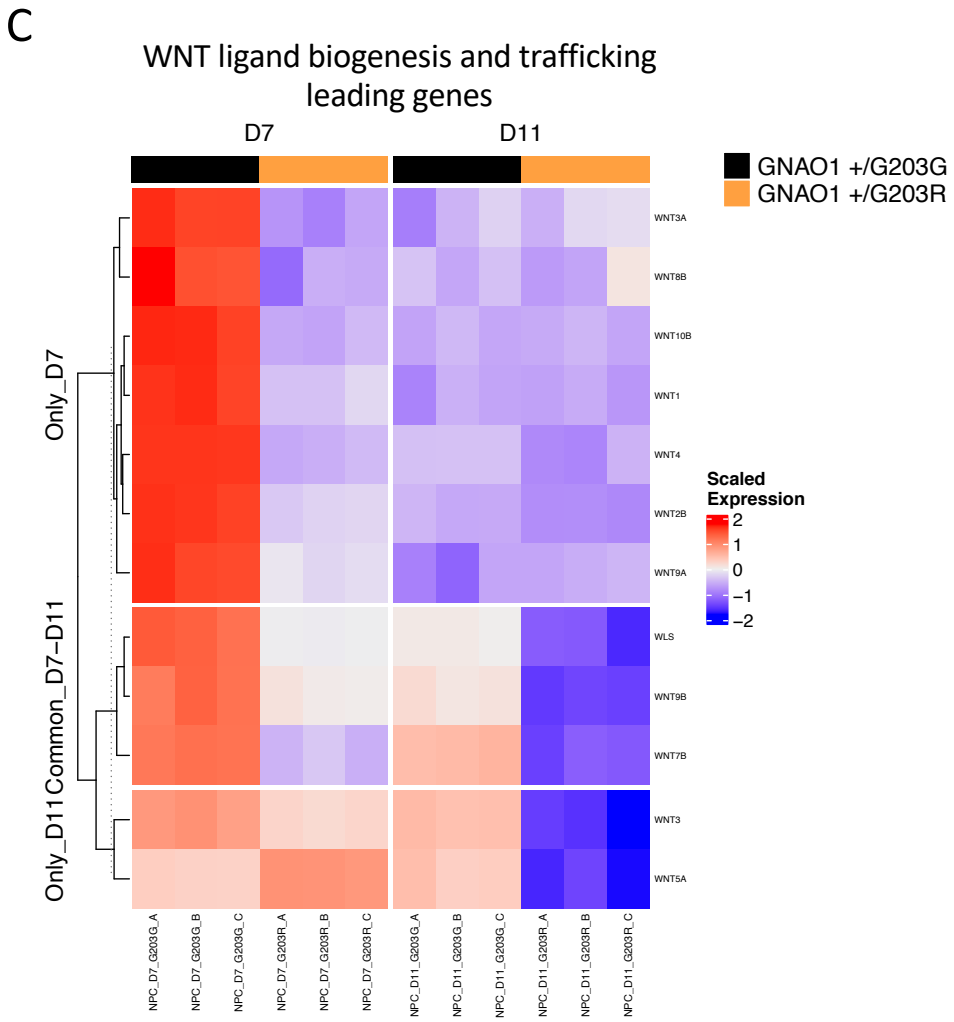
WNT ligand biogenesis and trafficking leading genes
D7
D11
GNAO1 +/G203G
GNAO1 +/G203R
Only_D7
Common_D7−D11
Only_D11
WNT3A
WNT8B
WNT10B
WNT1
WNT4
WNT2B
WNT9A
WLS
WNT9B
WNT7B
WNT3
WNT5A
NPC_D7_G203G_A
NPC_D7_G203G_B
NPC_D7_G203G_C
NPC_D7_G203R_A
NPC_D7_G203R_B
NPC_D7_G203R_C
NPC_D11_G203G_A
NPC_D11_G203G_B
NPC_D11_G203G_C
NPC_D11_G203R_A
NPC_D11_G203R_B
NPC_D11_G203R_C
Scaled Expression
2
1
0
−1
−2

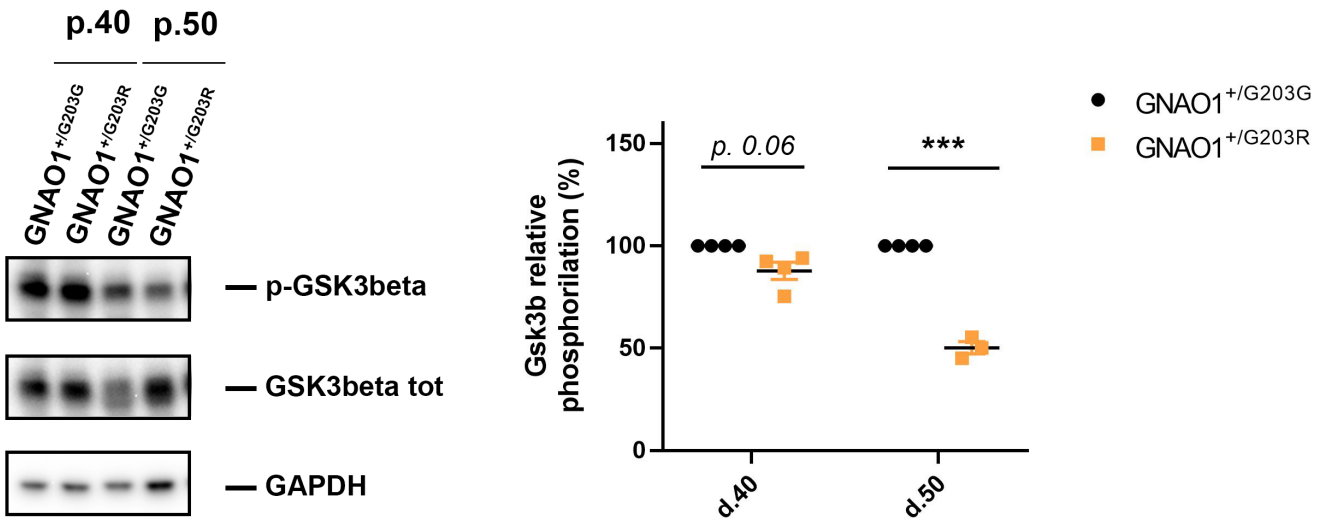
p.40
p.50
GNAO1+/G203G
GNAO1+/G203R
GNAO1+/G203G
GNAO1+/G203R
p-GSK3beta
GSK3beta tot
GAPDH
Gsk3b relative phosphorilation (%)
150
100
50
0
p. 0.06
***
d.40
d.50
GNAO1+/G203G
GNAO1+/G203R